arXiv:1612.07763v2 [math.OC] 23 Dec 2016

Optimizing the Kelvin force in a moving target subdomain *

Harbir Antil † Ricardo H. Nochetto ‡ Pablo Venegas §

March 10, 2022

Abstract In order to generate a desired Kelvin (magnetic) force in a target subdomain moving along a prescribed trajectory, we propose a minimization problem with a tracking type cost functional. We use the so-called dipole approximation to realize the magnetic field, where the location and the direction of the magnetic sources are assumed to be fixed. The magnetic field intensity acts as the control and exhibits limiting pointwise constraints. We address two specific problems: the first one corresponds to a fixed final time whereas the second one deals with an unknown force to minimize the final time. We prove existence of solutions and deduce local uniqueness provided that a second order sufficient condition is valid. We use the classical backward Euler scheme for time discretization. For both problems we prove the H^1-weak convergence of this semi-discrete numerical scheme. This result is motivated by Γ-convergence and does not require second order sufficient condition. If the latter holds then we prove H^1-strong local convergence. We report computational results to assess the performance of the numerical methods. As an application, we study the control of magnetic nanoparticles as those used in magnetic drug delivery, where the optimized Kelvin force is used to transport the drug to a desired location.

Key Words Magnetic field design, Kelvin force, minimization problem, non-convex problem, Γ-convergence.

AMS subject classification 65D05, 49J20, 49M25, 65M12, 65M60

*The work of H. Antil has been partially supported by NSF grants DMS-1109325 and DMS-1521590. R.H. Nochetto has been partially supported by NSF grants DMS-1109325 and DMS-1411808 and P. Venegas has been supported by NSF grant DMS-1411808 and CONICYT scholarship (Chile).

†Department of Mathematical Sciences. George Mason University, Fairfax, VA 22030, USA. Email: hantil@gmu.edu.

‡Department of Mathematics and Institute for Physical Science and Technology, University of Maryland College Park, MD 20742, USA. Email: rhn@math.umd.edu.

§GIMNAP, Departamento de Matemática, Universidad del Bío Bío, Chile. Email: pvenegas@ubiobio.cl.

1 Introduction

It is well-known that the magnetic field exerts a force on magnetic materials such as magnetic nanoparticles (MNPs). This principle has been widely exploited. For instance, MNPs under the action of external magnetic field are used in medical sciences: as contrast agents to enhance the contrast in MRI [6, 36], as carriers for targeted drug delivery [23, 27], to treat cancer and tumor cells in magnetic hyperthermia [17, 26], in gene therapy [9] and in magnetized stem-cells [35], among others. The application of magnetic force is not restricted to the medical sciences; these forces are relevant in magnetic tweezers [8, 16], lab-on-a-chip systems that include magnetic particles or fluids [12, 21], magnetofection [11, 33] or separation of particles [38, 22], just to name a few.

To understand how a magnetic field can manipulate MNPs, we need to recall that a magnetic field gradient is required to exert a force at a distance, such a magnetic force is given by [30]:

$$\boldsymbol{F} = (\boldsymbol{m} \cdot \nabla)\boldsymbol{H}, \tag{1.1}$$

where $\boldsymbol{m}$ is the magnetic dipole moment and $\boldsymbol{H}$ is the magnetic field. To address the computation of (1.1) we analyze the magnetic force acting on a point-like magnetic dipole. In the case of a magnetic nanoparticle suspended in a weakly diamagnetic medium such as water, the total moment on the particle can be written as $\boldsymbol{m} = V_m\boldsymbol{M}$, where V_m is the volume of the particle and $\boldsymbol{M}$ is its volumetric magnetization. In diamagnetic and paramagnetic materials, the relation between $\boldsymbol{M}$ and $\boldsymbol{H}$ is linear, which in turn is given by $\boldsymbol{M} = \Delta\chi\boldsymbol{H}$, where $\Delta\chi = \chi_p - \chi_m$ is the effective susceptibility, namely, the difference in magnetic susceptibility between the magnetic particle, χ_p, and its surrounding buffer or medium, χ_m. Furthermore, provided there are no time-varying electric fields or currents in the medium, we can apply the Maxwell equation $\mathbf{curl}\,\boldsymbol{H} = 0$ so that equation (1.1) becomes:

$$\boldsymbol{F} = \frac{V_m\Delta\chi}{2}\nabla|\boldsymbol{H}|^2 \tag{1.2}$$

where we have used the identity: $\nabla(\boldsymbol{H}\cdot\boldsymbol{H}) = 2\boldsymbol{H}\times(\mathbf{curl}\,\boldsymbol{H}) + 2(\boldsymbol{H}\cdot\nabla)\boldsymbol{H} = 2(\boldsymbol{H}\cdot\nabla)\boldsymbol{H}$. A similar expression has been considered, for instance, in a simplified version of ferrohydrodynamics equations [30, 31].

The immediate and fundamental difficulty in correlating the magnetic field with the physically observable forces exerted on the elementary magnetic entities (for instance, nanoparticle or ferrofluid) is that the magnetic field intensity $\boldsymbol{H}$ is not parallel to the magnetic force $\boldsymbol{F}$. Instead, it may take any direction relative to $\boldsymbol{F}$ depending on the spatial distribution of the magnetic field sources (or field gradients).

Due to the physics of magnetic fields and forces, the majority of magnetic application systems have been designed to pull in or attract therapeutic particles to target regions (see Figure 1 (left)). It is, however, also possible to use two or more magnets to "magnetically inject" nanoparticles (see Figure 1 (center and right)) particles [34] or to fully manipulate microrobots in wireless micromanipulation [20]. As we notice, the interaction of these dipoles generates a zone where the magnetic force is pointing outward (see region A, Figure 1 (right)). This field can push particles away from the dipole positions.

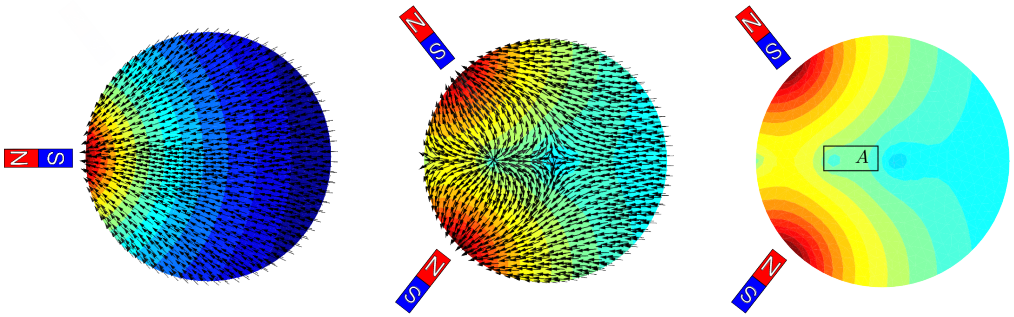


Figure 1: The panels show the magnetic force $\boldsymbol{F}$, with arrows indicating the normalized force direction generated using one and two permanent magnets. The background color indicates the magnetic force magnitude $|\nabla|\boldsymbol{H}|^2|$ on a log scale. In particular, the light and dark colors correspond to low and high values of $|\nabla|\boldsymbol{H}|^2|$. The left panel shows that using a permanent magnet one can generate $\boldsymbol{F}$ which can be used to pull in or attract particles to a region of interest. In contrast, using two permanent magnets we can generate $\boldsymbol{F}$ that enables us to "magnetically inject" particles. On the right panel (same as in the center without arrows), region A contains a zone where the arrows point to the right and thus enable pushing away from the magnets.

Indeed, the success of the aforementioned applications highly depend on the accurate control of the magnetic force. Such a control will enable us to better understand the existing and explore new applications of MNPs, ferrofluids and magnetic force-based models in general. In this paper we focus on a key question: how to approximate a desired magnetic force $\mathbf{f}$ by actuating a configuration of magnetic field sources whose location and direction are fixed. We aim to achieve this goal by studying a minimization problem

$$\min_{\boldsymbol{F}} \int_0^T \|\boldsymbol{F} - \mathbf{f}\|^2_{\mathrm{L}^2(D)}\, dt \quad \text{for } T > 0 \text{ and } D \subset \mathbb{R}^d, d = 2, 3.$$

A good approximation of $\mathbf{f}$ computed by the minimization problem enables us to manipulate, for instance, MNPs with the diversity of applications that this entails.

We begin this paper in Section 2 by discussing the mathematical formulation of two minimization problems. In Section 2.1, we assume that the final time T and the vector field $\mathbf{f}$ are given. In Section 2.2 we study the problem with an unknown vector field so as to minimize the final time T_F. To tackle this, we replace time with arc length. For both problems, we prove global existence and local uniqueness of minimizers, the latter provided a second order sufficient condition holds. Section 3 is devoted to the numerical analysis of the time-discrete problems. We obtain first a H^1-weak convergence, which is motivated by Γ-convergence. In addition, by assuming a second-order sufficient condition we prove H^1-strong local convergence for the first problem. In Section 4 we report numerical tests that assess the ability of both approaches to approximate spatially uniform vector fields in a moving subdomain and the performance of the corresponding

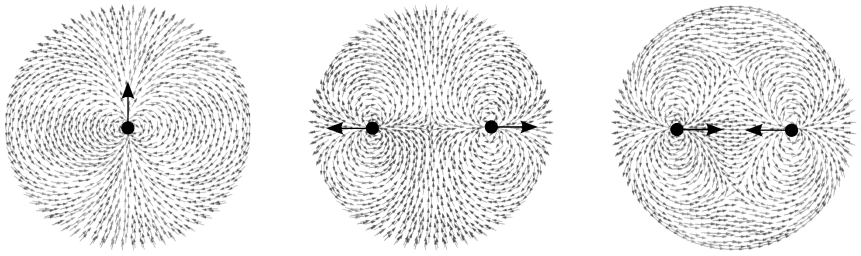


Figure 2: These panels depicts the magnetic field $\boldsymbol{H}$ (represented by small arrows) generated using the dipole approximation (2.2) for unit intensities ($\alpha_i = 1$, $i = 1, \ldots, n_p$). The i^{th} dipole is located at $\boldsymbol{x}_i \in \Omega$ with direction $\widehat{\boldsymbol{d}}_i$. Left panel: single dipole with $\widehat{\boldsymbol{d}}_1 = (0, 1)$ and $\boldsymbol{x}_1 = (0.0)$. Center panel: two dipoles with $\widehat{\boldsymbol{d}}_1 = (-1, 0)$, $\widehat{\boldsymbol{d}}_2 = (1, 0)$ and $\boldsymbol{x}_1 = (-0.5, 0)$, $\boldsymbol{x}_2 = (0.5, 0)$. Right panel: two dipoles with $\widehat{\boldsymbol{d}}_1 = (1, 0)$, $\widehat{\boldsymbol{d}}_2 = (-1, 0)$ and $\boldsymbol{x}_1 = (-0.5, 0)$, $\boldsymbol{x}_2 = (0.5, 0)$. For presentation purposes, we consider the normalized magnetic field on each example.

numerical schemes. We conclude with an example which illustrates how the optimal magnetic force, generated by the minimization problem, can be used in magnetic drug targeting.

2 Minimization and control

Let $\emptyset \subset \mathbb{R}^d$, $d = 2, 3$ be an open bounded domain and $T > 0$ be the final time. With D_t we denote a time dependent domain that deforms smoothly and is strictly contained in Ω for every $t \in [0, T]$. Our goal is then to approximate a vector field $\mathbf{f} \in [\mathrm{L}^2(0, T; \mathrm{L}^2(\Omega))]^d$ by the so–called Kelvin force (cf. (1.2)). We consider magnetic sources outside Ω, then, from the Maxwell equations it follows that the magnetic field $\boldsymbol{H}$ satisfies:

$$\mathbf{curl}\, \boldsymbol{H} = \mathbf{0}, \quad \mathrm{div}\, \boldsymbol{H} = 0 \quad \text{in } \Omega, \tag{2.1}$$

where the last equation follows by assuming a linear relation between the magnetic induction $\boldsymbol{B}$ and the magnetic field $\boldsymbol{H}$. The magnetic field generated by a current distribution and a permanent magnet can be modeled by the Biot-Savart law, which is a magnetostatic approximation. However, for simplicity, in our case we consider a dipole approximation to the magnet source (see Figure 2), which provides a concise and easily tractable representation of the magnetic field (see [29] for a quantification of the error associated with the dipole approximation). This approximation is commonly used for localization of objects in applications ranging from medical imaging to military. It is also extensively used in real-time control of magnetic devices in medical sciences [10, 25, 28]. In addition, fixed location and direction of magnetic dipoles but variable intensity field, is considered in several applications such as microrobots micromanipulation [20] or magnetic drug targeting [32]. With such a configuration it is possible to reduce the

numbers of free variables (fixed location and direction of dipoles) and the hardware involved.

Since we are interested in the feasibility of the field approximation rather than the optimality of the prescribed location, from now on we will assume that the magnetic field is modeled by the superposition of a fixed number n_p of dipoles, namely

$$\boldsymbol{H}(\boldsymbol{x},t)=\sum_{i=1}^{n_p}\alpha_i(t)\left(d\frac{(\boldsymbol{x}-\boldsymbol{x}_i)(\boldsymbol{x}-\boldsymbol{x}_i)^\top}{|\boldsymbol{x}-\boldsymbol{x}_i|^2}-\mathbb{I}\right)\frac{\widehat{\boldsymbol{d}}_i}{|\boldsymbol{x}-\boldsymbol{x}_i|^d}=\sum_{i=1}^{n_p}\alpha_i(t)\boldsymbol{H}_i(\boldsymbol{x}), \tag{2.2}$$

where $\mathbb{I}\in\mathbb{R}^{d\times d}$ is the identity matrix. In addition, $\widehat{\boldsymbol{d}}_i\in\mathbb{R}^d$ and $\boldsymbol{x}_i\in\mathbb{R}^d\setminus\overline{\emptyset}$, $i=1,\dots,n_p$, denote fixed unit vectors and dipole positions, respectively (see Figure 3). It is straightforward to show that the magnetic field given by (2.2) satisfies (2.1).

2.1 Problem 1: Fixed final time

With this configuration in mind, we introduce the minimization problem

$$\min_{\boldsymbol{\alpha}\in\mathcal{H}_{ad}}\mathcal{J}(\boldsymbol{\alpha}) \tag{2.3a}$$

with

$$\mathcal{J}(\boldsymbol{\alpha}):=\frac{1}{2}\int_0^T\|\nabla|\boldsymbol{H}(\boldsymbol{\alpha})|^2-\mathbf{f}\|^2_{\mathrm{L}^2(D_t)}dt+\frac{\lambda}{2}\int_0^T|d_t\boldsymbol{\alpha}|^2dt. \tag{2.3b}$$

Here $\boldsymbol{\alpha}(t):=(\alpha_1(t),\dots,\alpha_{n_p}(t))^\top\in\mathbb{R}^{n_p}$ denotes the vector of magnetic field intensities, and $\lambda>0$ is the cost of control. A nonzero λ in (2.3a) will enforce a smooth evolution of the intensities. Moreover, the larger the value of λ, the smoother is this evolution. For given constant vectors $\boldsymbol{\alpha}_0,\boldsymbol{\alpha}_*,\boldsymbol{\alpha}^*\in\mathbb{R}^{n_p}$, we seek $\boldsymbol{\alpha}$ in the following admissible convex set:

$$\mathcal{H}_{ad}:=\left\{\boldsymbol{\alpha}\in[\mathrm{H}^1(0,T)]^{n_p}:\boldsymbol{\alpha}(0)=\boldsymbol{\alpha}_0\quad\text{and}\quad\boldsymbol{\alpha}_*\le\boldsymbol{\alpha}(t)\le\boldsymbol{\alpha}^*,\ \forall t\in[0,T]\right\}. \tag{2.4}$$

Notice that the feasibility of the dipole approximation can be studied with the first term of $\mathcal{J}$. Applications of (2.3) include control of drug concentration, introducing particles containing nucleic acids into target cells (magnetofection), and to separate magnetic materials from a nonmagnetic liquid medium.

The resulting magnetic force arising as a solution to (2.3) can be used to control drug concentration, cell, or to separate magnetic materials from a nonmagnetic liquid medium, among other applications.

Remark 2.1. Changing the number of dipoles, their positions or magnetic field directions leads to different configurations for the minimization problem (2.3). Although the computed force may vary depending on the configuration, the following mathematical analysis remains the same.

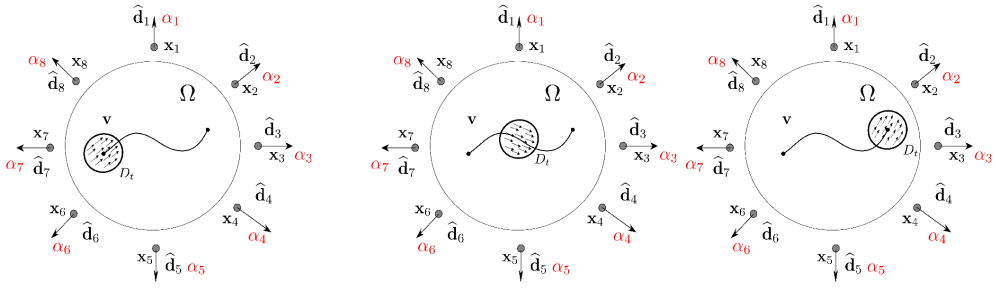


Figure 3: Configuration of $n_p = 8$ dipoles surrounding a computational domain $\Omega \subset \mathbb{R}^2$ and moving domain D_t. The target vector field $\mathbf{f}$, represented with arrows, is shown only in D_t. Each dipole is characterized by its position $\boldsymbol{x}_i$ (represented by a dot outside $\emptyset$), direction $\boldsymbol{d}_i$ (represented by an arrow) and the magnitude $\boldsymbol{\alpha}_i$, for $i = 1, \ldots, n_p$. The evolution of a circular moving domain D_t is shown for different times: $t = 0$ (left), $t \in (0, T)$ (center) and $t = T$ (right). The center of D_t moves along a curve represented by the solid line inside $\emptyset$.

In view of (2.2), we can rewrite $\boldsymbol{H}$ as

$$\boldsymbol{H}(\boldsymbol{x}, t) = \sum_{i=1}^{n_p} \alpha_i(t) \boldsymbol{H}_i(\boldsymbol{x}) = \mathbb{H}(\boldsymbol{x})\boldsymbol{\alpha}(t)$$

where $\mathbb{H} = \left(\boldsymbol{H}_1\, \boldsymbol{H}_2\, \ldots\, \boldsymbol{H}_{n_p}\right) \in [C^\infty(\overline{\Omega})]^{d \times n_p}$. Thus

$$\begin{aligned}\nabla |\boldsymbol{H}(\boldsymbol{x}, t)|^2 &= \nabla \left(\boldsymbol{\alpha}(t)^\top \mathbb{H}(\boldsymbol{x})^\top \mathbb{H}(\boldsymbol{x}) \boldsymbol{\alpha}(t) \right) \\ &= \begin{pmatrix} \boldsymbol{\alpha}(t)^\top \partial_{x_1} (\mathbb{H}(\boldsymbol{x})^\top \mathbb{H}(\boldsymbol{x})) \boldsymbol{\alpha}(t) \\ \vdots \\ \boldsymbol{\alpha}(t)^\top \partial_{x_d} (\mathbb{H}(\boldsymbol{x})^\top \mathbb{H}(\boldsymbol{x})) \boldsymbol{\alpha}(t) \end{pmatrix} = \begin{pmatrix} \boldsymbol{\alpha}^\top \boldsymbol{P}_1 \boldsymbol{\alpha} \\ \vdots \\ \boldsymbol{\alpha}^\top \boldsymbol{P}_d \boldsymbol{\alpha} \end{pmatrix}\end{aligned}$$

with $\boldsymbol{P}_i = \partial_{x_i}(\mathbb{H}^\top \mathbb{H}) \in [C^\infty(\overline{\Omega})]^{n_p \times n_p}, i = 1, \ldots, d$. If $\mathbf{f} := (\mathrm{f}_1, \ldots, \mathrm{f}_d)^\top$, then from the above equation we notice that (2.3a) reduces to

$$\min_{\boldsymbol{\alpha} \in \mathcal{H}_{ad}} \mathcal{J}(\boldsymbol{\alpha}), \quad \mathcal{J}(\boldsymbol{\alpha}) = \frac{1}{2} \int_0^T \left(\sum_{i=1}^{d} \| \boldsymbol{\alpha}^\top \boldsymbol{P}_i \boldsymbol{\alpha} - \mathrm{f}_i \|^2_{\mathrm{L}^2(D_t)} + \lambda |d_t \boldsymbol{\alpha}|^2 \right) dt. \tag{2.5}$$

Next, we focus on the mathematical analysis of the minimization problem (2.5), which is nonconvex. We first embark on a journey to show the existence and local uniqueness of a solution to (2.5). For notational simplicity, from now on we denote by V both a Banach space V and the Banach tensor product V^{n_p}.

Theorem 2.2 (existence of minimizers)**.** *There exist at least one solution* $\bar{\boldsymbol{\alpha}}$ *to the minimization problem* (2.5)*.*

Proof. We apply the direct method of the calculus of variations. Given that $\mathcal{J}$ is bounded below by zero, we deduce that $j = \inf_{\boldsymbol{\alpha}\in\mathcal{H}_{ad}} \mathcal{J}(\boldsymbol{\alpha})$ is finite. We can thus construct a minimizing sequence $\{\boldsymbol{\alpha}_n\}_{n\in\mathbb{N}}$ such that

$$j = \lim_{n\to\infty} \mathcal{J}(\boldsymbol{\alpha}_n).$$

As the sequence $\{\boldsymbol{\alpha}_n\}_{n\in\mathbb{N}}$ is uniformly bounded in $\mathcal{H}_{ad} \subset \mathrm{H}^1(0,T)$, we can extract a (not relabeled) weakly convergent subsequence $\{\boldsymbol{\alpha}_n\}_{n\in\mathbb{N}}$ such that

$$\boldsymbol{\alpha}_n \rightharpoonup \bar{\boldsymbol{\alpha}} \quad \text{in } \mathrm{H}^1(0,T), \qquad \bar{\boldsymbol{\alpha}} \in \mathcal{H}_{ad}. \tag{2.6}$$

Moreover, according to [3, Theorem 9.16] we have

$$\boldsymbol{\alpha}_n \to \bar{\boldsymbol{\alpha}} \quad \text{in } C([0,T]). \tag{2.7}$$

To show the optimality of $\bar{\boldsymbol{\alpha}}$, we first consider (2.7) to get that

$$\int_0^T \|\boldsymbol{\alpha}_n^\top \boldsymbol{P}_i \boldsymbol{\alpha}_n - \mathrm{f}_i\|^2_{\mathrm{L}^2(D_t)} \to \int_0^T \|\bar{\boldsymbol{\alpha}}^\top \boldsymbol{P}_i \bar{\boldsymbol{\alpha}} - \mathrm{f}_i\|^2_{\mathrm{L}^2(D_t)} \qquad i = 1, \dots, d.$$

This and the fact that the last term in $\mathcal{J}$ is weakly lower semicontinuous (see [37, Theorem 2.12]) yields

$$\min_{\boldsymbol{\alpha}\in\mathcal{H}_{ad}} \mathcal{J}(\boldsymbol{\alpha}) = \liminf_{n\to\infty} \mathcal{J}(\boldsymbol{\alpha}_n) \geq \mathcal{J}(\bar{\boldsymbol{\alpha}}),$$

which concludes the proof. □

We now state the first order optimality condition. This follows by standard arguments (see [37, Lemma 2.21]) in view of the fact that $\mathcal{J} : \mathrm{H}^1(0,T) \to \mathbb{R}$ is Fréchet differentiable.

Lemma 2.3 (first order optimality condition)**.** *If $\bar{\boldsymbol{\alpha}} \in \mathcal{H}_{ad}$ denotes an optimal control, given by Theorem 2.2, then the first order necessary optimality condition satisfied by $\bar{\boldsymbol{\alpha}}$ is*

$$\mathcal{J}'(\bar{\boldsymbol{\alpha}}) \langle \boldsymbol{\alpha} - \bar{\boldsymbol{\alpha}} \rangle \geq 0 \qquad \forall \boldsymbol{\alpha} \in \mathcal{H}_{ad}$$

where, for $\delta\boldsymbol{\alpha} = (\boldsymbol{\alpha} - \bar{\boldsymbol{\alpha}})$ we have

$$\mathcal{J}'(\bar{\boldsymbol{\alpha}}) \langle \delta\boldsymbol{\alpha} \rangle = \int_0^T \left(\sum_{i=1}^d \int_{D_t} \left(\bar{\boldsymbol{\alpha}}^\top \boldsymbol{P}_i \bar{\boldsymbol{\alpha}} - \mathrm{f}_i \right) \left(2\bar{\boldsymbol{\alpha}}^\top \boldsymbol{P}_i \delta\boldsymbol{\alpha} \right) d\boldsymbol{x} + \lambda d_t \bar{\boldsymbol{\alpha}}^\top d_t \delta\boldsymbol{\alpha} \right) dt.$$

Since $\mathcal{J}$ is nonconvex, it is customary (cf. [37, Section 4.10]) to assume that $\bar{\boldsymbol{\alpha}}$ is a nondegenerate local minimizer, namely that there exists $\omega > 0$ such that

$$\mathcal{J}''(\bar{\boldsymbol{\alpha}}) \langle \delta\boldsymbol{\alpha}, \delta\boldsymbol{\alpha} \rangle \geq \omega |\delta\boldsymbol{\alpha}|^2_{\mathrm{H}^1(0,T)} \qquad \forall \delta\boldsymbol{\alpha} \in \mathcal{A}(\bar{\boldsymbol{\alpha}}) \tag{2.8}$$

where

$$\begin{aligned}&\mathcal{J}''(\bar{\boldsymbol{\alpha}})\,\langle\delta\boldsymbol{\alpha},\delta\boldsymbol{\alpha}\rangle\\&\quad=2\int_0^T\int_{D_t}\sum_{i=1}^{d}\left(\left(\bar{\boldsymbol{\alpha}}^\top\boldsymbol{P}_i\bar{\boldsymbol{\alpha}}-\mathrm{f}_i\right)(\delta\boldsymbol{\alpha})^\top\boldsymbol{P}_i(\delta\boldsymbol{\alpha})+2\left(\bar{\boldsymbol{\alpha}}^\top\boldsymbol{P}_i\delta\boldsymbol{\alpha}\right)^2\right)+\lambda\int_0^T|d_t(\delta\boldsymbol{\alpha})|^2\end{aligned}$$

and

$$\mathcal{A}(\boldsymbol{\alpha}):=\left\{\boldsymbol{h}\in\mathrm{H}^1(0,T):\boldsymbol{h}(0)=\boldsymbol{0},\ \boldsymbol{\alpha}+\zeta\boldsymbol{h}\in\mathcal{H}_{ad},\ \forall 0\le\zeta\le 1\right\}$$

is the set of admissible variations of $\boldsymbol{\alpha}\in\mathcal{H}_{ad}$. This ensures local uniqueness as we show now.

Lemma 2.4 (local uniqueness)**.** *If $\bar{\boldsymbol{\alpha}}\in\mathcal{H}_{ad}$ solves* (2.5) *and satisfies* (2.8)*, then there exist positive constants ν and $\hat{C}$ such that for all $\boldsymbol{\alpha}\in\mathcal{H}_{ad}$ with $\|\boldsymbol{\alpha}-\bar{\boldsymbol{\alpha}}\|_{\mathrm{L}^2(0,T)}\le\nu$*

$$\mathcal{J}(\boldsymbol{\alpha})\ge\mathcal{J}(\bar{\boldsymbol{\alpha}})+\hat{C}\|\boldsymbol{\alpha}-\bar{\boldsymbol{\alpha}}\|^2_{\mathrm{H}^1(0,T)}.\tag{2.9}$$

Proof. It is easy to see that $\mathcal{J}:\mathrm{H}^1(0,T)\to\mathbb{R}$ is twice continuously Fréchet differentiable. Thus, from Taylor's theorem we have that there exists $\xi\in(0,1)$ such that for all $\delta\boldsymbol{\alpha}:=\boldsymbol{\alpha}-\bar{\boldsymbol{\alpha}}\in\mathcal{A}(\bar{\boldsymbol{\alpha}})$

$$\begin{aligned}\mathcal{J}(\boldsymbol{\alpha})=\mathcal{J}(\bar{\boldsymbol{\alpha}})+\mathcal{J}'(\bar{\boldsymbol{\alpha}})\,\langle\delta\boldsymbol{\alpha}\rangle+\frac{1}{2}\mathcal{J}''(\bar{\boldsymbol{\alpha}})\,\langle\delta\boldsymbol{\alpha},\delta\boldsymbol{\alpha}\rangle\\+\frac{1}{2}\left(\mathcal{J}''(\bar{\boldsymbol{\alpha}}+\xi(\delta\boldsymbol{\alpha}))-\mathcal{J}''(\bar{\boldsymbol{\alpha}})\right)\langle\delta\boldsymbol{\alpha},\delta\boldsymbol{\alpha}\rangle\,.\end{aligned}$$

Next, we estimate the last term on the right-hand side of the above equation. With this in mind, for $\boldsymbol{\alpha}_1:=\bar{\boldsymbol{\alpha}}+\xi(\delta\boldsymbol{\alpha})$ and $\boldsymbol{\alpha}_2:=\bar{\boldsymbol{\alpha}}$ we consider

$$\begin{aligned}&\left(\mathcal{J}''(\boldsymbol{\alpha}_1)-\mathcal{J}''(\boldsymbol{\alpha}_2)\right)\langle\delta\boldsymbol{\alpha},\delta\boldsymbol{\alpha}\rangle\\&=2\int_0^T\int_{D_t}\sum_{i=1}^{d}\Bigg(\left(\boldsymbol{\alpha}_1^\top\boldsymbol{P}_i\boldsymbol{\alpha}_1-\boldsymbol{\alpha}_2^\top\boldsymbol{P}_i\boldsymbol{\alpha}_2\right)(\delta\boldsymbol{\alpha})^\top\boldsymbol{P}_i\delta\boldsymbol{\alpha}\\&\quad+2\left(\left(\boldsymbol{\alpha}_1^\top\boldsymbol{P}_i\delta\boldsymbol{\alpha}\right)^2-\left(\boldsymbol{\alpha}_2^\top\boldsymbol{P}_i\delta\boldsymbol{\alpha}\right)^2\right)\Bigg)\\&=2\int_0^T\int_{D_t}\sum_{i=1}^{d}\left(\boldsymbol{\alpha}_1^\top\boldsymbol{P}_i(\boldsymbol{\alpha}_1-\boldsymbol{\alpha}_2)+\boldsymbol{\alpha}_2^\top\boldsymbol{P}_i(\boldsymbol{\alpha}_1-\boldsymbol{\alpha}_2)\right)(\delta\boldsymbol{\alpha})^\top\boldsymbol{P}_i\delta\boldsymbol{\alpha}\\&\quad+4\int_0^T\int_{D_t}\sum_{i=1}^{d}\left((\boldsymbol{\alpha}_1-\boldsymbol{\alpha}_2)^\top\boldsymbol{P}_i\delta\boldsymbol{\alpha}\right)\left((\boldsymbol{\alpha}_1+\boldsymbol{\alpha}_2)^\top\boldsymbol{P}_i\delta\boldsymbol{\alpha}\right).\end{aligned}$$

A simple application of Cauchy-Schwarz inequality in conjunction with the embedding

$\mathrm{H}^1(0,T) \subset C([0,T])$ leads to

$$\begin{aligned}
&\Big(\mathcal{J}''(\boldsymbol{\alpha}_1) - \mathcal{J}''(\boldsymbol{\alpha}_2)\Big)\,\langle \delta\boldsymbol{\alpha}, \delta\boldsymbol{\alpha}\rangle \\
&\quad \leq 2\|\boldsymbol{\alpha}_1 - \boldsymbol{\alpha}_2\|_{\mathrm{L}^2(0,T)}\|\delta\boldsymbol{\alpha}\|^2_{C(0,T)}|D_t|\Big(\sum_{i=1}^d \|P_i\|^2_{\mathrm{L}^\infty(\emptyset)}\Big)\Big(\|\boldsymbol{\alpha}_1\|_{\mathrm{L}^2(0,T)} + \|\boldsymbol{\alpha}_2\|_{\mathrm{L}^2(0,T)}\Big) \\
&\qquad + 4\|\boldsymbol{\alpha}_1 - \boldsymbol{\alpha}_2\|_{\mathrm{L}^2(0,T)}\|\delta\boldsymbol{\alpha}\|^2_{C(0,T)}|D_t|\Big(\sum_{i=1}^d \|P_i\|^2_{\mathrm{L}^\infty(\emptyset)}\Big)\|\boldsymbol{\alpha}_1 + \boldsymbol{\alpha}_2\|_{\mathrm{L}^2(0,T)} \\
&\quad \leq C_1\|\boldsymbol{\alpha}_1 - \boldsymbol{\alpha}_2\|_{\mathrm{L}^2(0,T)}\|\delta\boldsymbol{\alpha}\|^2_{\mathrm{H}^1(0,T)}
\end{aligned}$$

where we used the fact that D_t is a subset of Ω for all $t \in [0,T]$. From the above inequality and (2.8) it follows that

$$\mathcal{J}(\boldsymbol{\alpha}) \geq \mathcal{J}(\bar{\boldsymbol{\alpha}}) + \mathcal{J}'(\bar{\boldsymbol{\alpha}})\,\langle \delta\boldsymbol{\alpha}\rangle + \frac{\omega}{2}|\delta\boldsymbol{\alpha}|^2_{\mathrm{H}^1(0,T)} - \frac{C_1}{2}\|\delta\boldsymbol{\alpha}\|_{\mathrm{L}^2(0,T)}\|\delta\boldsymbol{\alpha}\|^2_{\mathrm{H}^1(0,T)}.$$

Then, the assertion follows from the first-order optimality condition (cf. Lemma 2.3) and the norm equivalence in $\mathcal{A}(\bar{\boldsymbol{\alpha}})$ provided that $\|\delta\boldsymbol{\alpha}\|_{\mathrm{L}^2(0,T)} \leq \nu$ for ν small enough. □

Remark 2.5 (sufficient condition for (2.8))**.** The second derivative of $\mathcal{J}(\bar{\boldsymbol{\alpha}})$ in the direction $\delta\boldsymbol{\alpha} \in \mathcal{A}(\bar{\boldsymbol{\alpha}})$ can be estimated by using the Sobolev embedding $\mathrm{H}^1(0,T) \subset C([0,T])$ and $\|\delta\boldsymbol{\alpha}\|_{C([0,T])} \leq T^{1/2}|\delta\boldsymbol{\alpha}|_{\mathrm{H}^1(0,T)}$ as follows

$$\begin{aligned}
\mathcal{J}''(\bar{\boldsymbol{\alpha}})\,\langle \delta\boldsymbol{\alpha}, \delta\boldsymbol{\alpha}\rangle \geq -2|D_t|\sum_{i=1}^d \Big(&\|\bar{\boldsymbol{\alpha}}^\top \boldsymbol{P}_i\bar{\boldsymbol{\alpha}}\|_{\mathrm{L}^\infty(0,T;\mathrm{L}^\infty(D_t))}\|\boldsymbol{P}_i\|_{\mathrm{L}^\infty(\emptyset)} \\
&+ 2\|\bar{\boldsymbol{\alpha}}\|^2_{\mathrm{L}^\infty(0,T)}\|\boldsymbol{P}_i\|^2_{\mathrm{L}^\infty(\emptyset)}\Big)\|\delta\boldsymbol{\alpha}\|^2_{\mathrm{L}^2(0,T)} \\
&- 2T|\delta\boldsymbol{\alpha}|^2_{\mathrm{H}^1(0,T)}\sum_{i=1}^d \|\mathrm{f}_i\|_{\mathrm{L}^1(0,T;\mathrm{L}^1(D_t))}\|\boldsymbol{P}_i\|_{\mathrm{L}^\infty(\emptyset)} + \lambda|\delta\boldsymbol{\alpha}|^2_{\mathrm{H}^1(0,T)}.
\end{aligned} \tag{2.10}$$

The celebrated Poincaré inequality $\|\delta\boldsymbol{\alpha}\|_{\mathrm{L}^2(0,T)} \leq T|\delta\boldsymbol{\alpha}|_{\mathrm{H}^1(0,T)}$ yields

$$\begin{aligned}
\mathcal{J}''(\bar{\boldsymbol{\alpha}})\,\langle \delta\boldsymbol{\alpha}, \delta\boldsymbol{\alpha}\rangle \geq \Bigg(\lambda - 2\sum_{i=1}^d \Big(&3T^2|D_t|\|\boldsymbol{P}_i\|^2_{\mathrm{L}^\infty(\emptyset)}\|\bar{\boldsymbol{\alpha}}\|^2_{\mathrm{L}^\infty(0,T)} \\
&+ T|D_t|^{1/2}\|\mathrm{f}_i\|_{\mathrm{L}^1(0,T;\mathrm{L}^2(D_t))}\|\boldsymbol{P}_i\|_{\mathrm{L}^\infty(\emptyset)}\Big)\Bigg)|\delta\boldsymbol{\alpha}|^2_{\mathrm{H}^1(0,T)}.
\end{aligned}$$

Clearly, a sufficient condition for (2.8) to hold is to consider λ sufficiently big which, however, is not reasonable for applications. Another condition for such an inequality to hold is take either T or D_t small enough. Practically speaking, this appears in [8, 16].

We have so far approximated a fixed vector field $\mathbf{f}$. It is also meaningful to minimize the final time T_F. One way to realize this is by treating $\mathbf{f}$ as an unknown. This is the topic of discussion for the next section.

2.2 Problem 2: Minimizing the final time

For obvious reasons, an important quantity to account for is the time it takes for D_t to arrive at its final destination. This is, for instance, the scenario of magnetic drug targeting. This can be modeled by adding an unknown final time in the cost functional.

Notice that, in the previous section, magnetic force $\mathbf{f}$ and the moving domain D_t are not necessarily related. However, if the final time is an unknown, then a fixed vector field $\mathbf{f}$ in (2.5) is not a meaningful quantity. We are now interested in the "force" of D_t, an unknown quantity, to be considered as a part of the minimization problem. To properly handle the new unknown T_F, motivated by [19], we will reformulate the minimization problem in terms of the arc length. Such a reformulation enables us to replace the variable final time T_F by a fixed arc length s_F. As an additional modeling approximation, we assume that there exist a curve $\mathcal{C}$ (sufficiently smooth) with end points $(\boldsymbol{x}_I)$ and $(\boldsymbol{x}_F)$ that lies in $\emptyset$ (see Figure 4). We also assume that the displacement of D_t is characterized by $\boldsymbol{x}_C(t)$ which moves along $\mathcal{C}$ with velocity $d_t\boldsymbol{x}_C$, for instance, $D_t = \widehat{D} + \boldsymbol{x}_C(t)$, where $\widehat{D}$ is a reference domain. In order to minimize the final time

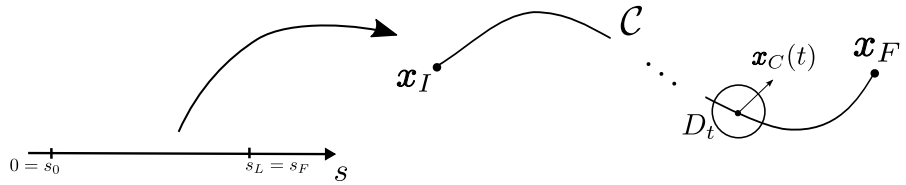


Figure 4: Two dimensional curve $\mathcal{C}$ and moving domain D_t with barycenter $\boldsymbol{x}_C$. The domain D_t travels along $\mathcal{C}$ from an initial point $\boldsymbol{x}_I$ to a final point $\boldsymbol{x}_F$.

$T_F > 0$, i.e, to maximize $d_t\boldsymbol{x}_C$ we introduce $s \in [0, s_F]$ which represents the arc length parameter of the curve $\mathcal{C}$. We assume that $\boldsymbol{x}_C(t)$ starts from $\boldsymbol{x}_I$ at $t = 0$ and moves along $\mathcal{C}$ with an arbitrary speed $\theta(t) > 0$, and eventually reaches $\boldsymbol{x}_F$ at $t = T_F$. With this in mind, we define a map $\sigma(\cdot) : [0, T_F] \to [0, s_F]$ as

$$s = \sigma(t) = \int_0^t \theta(\tau) d\tau. \tag{2.11}$$

Moreover, we assume that there exists a parametrization $\boldsymbol{\rho}$ of $\mathcal{C}$ depending on the arc length $s \in [0, s_F]$ such that $\boldsymbol{x}_C(\cdot) = \boldsymbol{\rho} \circ \sigma(\cdot)$. In the sequel we will assume that $\boldsymbol{\rho} \in C^1[0, s_F]$. From the above and by setting $\boldsymbol{\rho}' = d_t\boldsymbol{\rho}$ we arrive at $d_t\boldsymbol{x}_C(t) = \theta(t)\boldsymbol{\rho}'(\sigma(t))$. We assume that the vector $d_t\boldsymbol{x}_C(t)$ has units similar to $\boldsymbol{F}$. As in Problem 1, we consider a tracking type term:

$$\int_0^{T_F} \left(\frac{1}{2} \sum_{i=1}^{d} \| \boldsymbol{\alpha}(\sigma(t))^\top \boldsymbol{P}_i \boldsymbol{\alpha}(\sigma(t)) - d_t \boldsymbol{x}_{i,C}(t) \|^2_{\mathrm{L}^2(D_{\sigma(t)})} + \beta \right) dt, \tag{2.12}$$

where $\beta > 0$ is an additional penalty parameter and $\boldsymbol{x}_C := (\boldsymbol{x}_{1,C}, \ldots, \boldsymbol{x}_{d,C})^\top$. The last term on the right hand side of (2.12) is related with the minimization of the final time:

the larger the value of β, the smaller the value of T_F. Notice that $\boldsymbol{\alpha} : [0, s_F] \to \mathbb{R}$ and the moving domain are defined in terms of arc length s and are thus independent of θ. It is easy to see that the intent of (2.12) is to approximate $d_t \boldsymbol{x}_C$ and minimize the final time T_F. However, as we notice in the previous section, another important consideration of the minimization problem is to control the rate of change of the variables involved. With this in mind, we apply the change of variables (2.11) in (2.12) and propose the minimization problem:

$$\min_{(\boldsymbol{\alpha},\theta)\in\mathcal{U}_{ad}\times\mathcal{V}_{ad}} \mathcal{F}(\boldsymbol{\alpha},\theta) \tag{2.13a}$$

with

$$\begin{aligned}\mathcal{F}(\boldsymbol{\alpha},\theta) := \int_0^{s_F} \Bigg(& \frac{1}{2\theta(s)} \sum_{i=1}^{d} \|\boldsymbol{\alpha}(s)^\top \boldsymbol{P}_i \boldsymbol{\alpha}(s) - \boldsymbol{\rho}_i'(s)\theta(s)\|^2_{\mathrm{L}^2(D_s)} \\ & + \frac{\beta}{\theta(s)} + \frac{\lambda}{2}|d_s\boldsymbol{\alpha}(s)|^2 + \frac{\eta}{2}|d_s\theta(s)|^2 \Bigg) ds\end{aligned} \tag{2.13b}$$

where, for notational simplicity, we have used $\theta(\cdot) := \theta \circ \sigma^{-1}(\cdot)$. In the above functional we have considered additional regularization terms: for $\lambda, \eta > 0$, the last two term in (2.13b) will enforce a smooth evolution of the intensities and velocity. The admissible sets for $\boldsymbol{\alpha}$ and θ are defined as

$$\begin{aligned}\mathcal{U}_{ad} &:= \left\{ \boldsymbol{\alpha} \in \mathrm{H}^1(0, s_F) : \boldsymbol{\alpha}(0) = \boldsymbol{\alpha}_0 \quad \text{and} \quad \boldsymbol{\alpha}_* \le \boldsymbol{\alpha}(s) \le \boldsymbol{\alpha}^*, \ \forall s \in [0, s_F] \right\}, \\ \mathcal{V}_{ad} &:= \left\{ \theta \in \mathrm{H}^1(0, s_F) : \theta(0) = \theta_0 \quad \text{and} \quad 0 < \theta_* \le \theta(s) \le \theta^*, \ \forall s \in [0, s_F] \right\}.\end{aligned}$$

Notice that, for fixed upper and lower bounds on the dipole intensities ($\boldsymbol{\alpha}^*$ and $\boldsymbol{\alpha}_*$, respectively) the maximum value of the magnetic force is fixed, thus, the maximum "velocity" is fixed. However, from practical considerations we may impose an upper bound θ^* lower than a physically reachable velocity obtained for a given pair $(\boldsymbol{\alpha}_*, \boldsymbol{\alpha}^*)$.

Theorem 2.6 (existence of minimizers)**.** *There exists at least one solution* $(\bar{\boldsymbol{\alpha}}, \bar{\theta})$ *to the control problem* (2.13a)*.*

Proof. The proof is similar to Theorem 2.2. Since $\mathcal{F}$ is bounded below by zero there exists a minimizing sequence $\{(\boldsymbol{\alpha}_n, \theta_n)\}_{n\in\mathbb{N}}$ such that

$$j := \inf_{(\boldsymbol{\alpha},\theta)\in\mathcal{U}_{ad}\times\mathcal{V}_{ad}} \mathcal{F}(\boldsymbol{\alpha},\theta) = \lim_{n\to\infty} \mathcal{F}(\boldsymbol{\alpha}_n, \theta_n)$$

which is uniformly bounded in $\mathcal{U}_{ad} \times \mathcal{V}_{ad} \subset [\mathrm{H}^1(0, s_F)]^2$. Hence there exists $(\bar{\boldsymbol{\alpha}}, \bar{\theta}) \in [\mathrm{H}^1(0, s_F)]^2$ such that $(\boldsymbol{\alpha}_n, \theta_n) \rightharpoonup (\bar{\boldsymbol{\alpha}}, \bar{\theta})$ in $\mathrm{H}^1(0, s_F)$ and $(\boldsymbol{\alpha}_n, \theta_n) \to (\bar{\boldsymbol{\alpha}}, \bar{\theta})$ in $C([0, s_F])$. We thus arrive at

$$\begin{gathered}\frac{1}{\theta_n^{1/2}} \left(\boldsymbol{\alpha}_n^\top \boldsymbol{P}_i \boldsymbol{\alpha}_n - \boldsymbol{\rho}_i' \theta_n \right) \to \frac{1}{\bar{\theta}^{1/2}} \left(\bar{\boldsymbol{\alpha}}^\top \boldsymbol{P}_i \bar{\boldsymbol{\alpha}} - \boldsymbol{\rho}_i' \bar{\theta} \right) \quad \text{in } \mathrm{L}^2(0, s_F; \mathrm{L}^2(D_s)) \\ \frac{\beta}{\theta_n} \to \frac{\beta}{\bar{\theta}} \quad \text{in } \mathrm{L}^2(0, s_F).\end{gathered}$$

This combined with the weak lower semicontinuity property of the $\mathrm{H}^1(0, s_F)$-semi-norm yields

$$\min_{(\boldsymbol{\alpha},\theta)\in\mathcal{U}_{ad}\times\mathcal{V}_{ad}} \mathcal{F}(\boldsymbol{\alpha},\theta) \geq \liminf_{n\to\infty} \mathcal{F}(\boldsymbol{\alpha}_n,\theta_n) \geq \mathcal{F}(\bar{\boldsymbol{\alpha}},\bar{\theta}).$$

This completes the proof. □

Before showing a local uniqueness result of problem (2.13a), we state the first order optimality condition which follows from the Fréchet differentiability of $\mathcal{F} : \mathrm{H}^1(0, s_F) \times \mathrm{H}^1(0, s_F) \to \mathbb{R}$.

Lemma 2.7 (first order optimality condition)**.** *If $(\bar{\boldsymbol{\alpha}}, \bar{\theta}) \in \mathcal{U}_{ad} \times \mathcal{V}_{ad}$ denotes an optimal control, given by Theorem 2.6, then the first order necessary optimality condition satisfied by $(\bar{\boldsymbol{\alpha}}, \bar{\theta})$ is*

$$\mathcal{F}'(\bar{\boldsymbol{\alpha}}, \bar{\theta}) \left\langle (\delta\boldsymbol{\alpha}, \delta\theta) \right\rangle \geq 0 \qquad \forall (\boldsymbol{\alpha}, \theta) \in \mathcal{U}_{ad} \times \mathcal{V}_{ad} \tag{2.14}$$

where $\delta\boldsymbol{\alpha} = \boldsymbol{\alpha} - \bar{\boldsymbol{\alpha}}$, $\delta\theta = \theta - \bar{\theta}$ and

$$\begin{aligned}
&\mathcal{F}'(\bar{\boldsymbol{\alpha}}, \bar{\theta}) \left\langle (\delta\boldsymbol{\alpha}, \delta\theta) \right\rangle \\
&\quad = \int_0^{s_F} \int_{D_s} \left(\sum_{i=1}^{d} \left(\frac{\bar{\boldsymbol{\alpha}}^\top \boldsymbol{P}_i \bar{\boldsymbol{\alpha}}}{\bar{\theta}^{1/2}} - \boldsymbol{\rho}_i' \bar{\theta}^{1/2} \right) \left(2\frac{\bar{\boldsymbol{\alpha}}^\top \boldsymbol{P}_i \delta\boldsymbol{\alpha}}{\bar{\theta}^{1/2}} - \frac{\bar{\boldsymbol{\alpha}}^\top \boldsymbol{P}_i \bar{\boldsymbol{\alpha}} \delta\theta}{2\bar{\theta}^{3/2}} - \frac{\boldsymbol{\rho}_i' \delta\theta}{2\bar{\theta}^{1/2}} \right) \right. \\
&\qquad \left. - \frac{\beta\delta\theta}{\bar{\theta}^2} + \lambda d_s \bar{\boldsymbol{\alpha}}^\top d_s \delta\boldsymbol{\alpha} + \eta d_s \bar{\theta} d_s \delta\theta \right) d\boldsymbol{x} ds.
\end{aligned}$$

Given that the functional $\mathcal{F}$ is non-convex, like in Problem 1, the following second order sufficient condition guarantees that $(\bar{\boldsymbol{\alpha}}, \bar{\theta})$ is a nondegenerate local minimizer: for all $(\boldsymbol{\alpha}, \theta) \in \mathcal{U}_{ad} \times \mathcal{V}_{ad}$, there exists $\tilde{\omega} > 0$ such that $\forall (\delta\boldsymbol{\alpha}, \delta\theta) \in \mathcal{B}(\bar{\boldsymbol{\alpha}}, \bar{\theta})$

$$\mathcal{F}''(\bar{\boldsymbol{\alpha}}, \bar{\theta}) \left\langle (\delta\boldsymbol{\alpha}, \delta\theta), (\delta\boldsymbol{\alpha}, \delta\theta) \right\rangle \geq \tilde{\omega} \left(\|\delta\theta\|^2_{\mathrm{H}^1(0,s_F)} + \|\delta\boldsymbol{\alpha}\|^2_{\mathrm{H}^1(0,s_F)} \right), \tag{2.15}$$

where

$$\begin{aligned}
\mathcal{B}(\boldsymbol{\alpha}, \theta) := \Big\{ (\boldsymbol{h}, \widehat{\theta}) \in [\mathrm{H}^1(0,T)]^2 : (\boldsymbol{h}(0), \widehat{\theta}(0)) = (0,0), \\
(\boldsymbol{\alpha}, \theta) + \zeta(\boldsymbol{h}, \widehat{\theta}) \in \mathcal{U}_{ad} \times \mathcal{V}_{ad},\ \forall \zeta \in [0,1] \Big\},
\end{aligned}$$

is the set of admissible variations of $(\boldsymbol{\alpha}, \theta) \in \mathcal{U}_{ad} \times \mathcal{V}_{ad}$. Consequently, the following lemma, yields the local uniqueness of problem (2.13a).

Lemma 2.8 (local uniqueness)**.** *If $(\bar{\boldsymbol{\alpha}}, \bar{\theta}) \in \mathcal{U}_{ad} \times \mathcal{V}_{ad}$ satisfy the first and second-order optimality conditions* (2.14) *and* (2.15)*, then there exist $\tilde{\nu}$ and $\hat{C}$ such that*

$$\mathcal{F}(\boldsymbol{\alpha}, \theta) \geq \mathcal{F}(\bar{\boldsymbol{\alpha}}, \bar{\theta}) + \hat{C} \left(\|\boldsymbol{\alpha} - \bar{\boldsymbol{\alpha}}\|^2_{\mathrm{H}^1(0,s_F)} + \|\theta - \bar{\theta}\|^2_{\mathrm{H}^1(0,s_F)} \right) \qquad \forall (\boldsymbol{\alpha}, \theta) \in \mathcal{U}_{ad} \times \mathcal{V}_{ad} \tag{2.16}$$

with $\|\boldsymbol{\alpha} - \bar{\boldsymbol{\alpha}}\|_{\mathrm{H}^1(0,s_F)} + \|\theta - \bar{\theta}\|_{\mathrm{H}^1(0,s_F)} \leq \tilde{\nu}$.

Proof. The estimate (2.16) follows by using the same techniques as in Lemma 2.4, namely, Taylor's expansion, first and second-order optimality conditions (2.14) and (2.15), and the following inequality: for $(\boldsymbol{\alpha}, \theta)$ and $(\boldsymbol{\alpha}_i, \theta_i) \in \mathcal{U}_{ad} \times \mathcal{V}_{ad}$, $i = 1, 2$,

$$\begin{aligned}\big(\mathcal{F}''(\boldsymbol{\alpha}_1, \theta_1) - \mathcal{F}''(\boldsymbol{\alpha}_2, \theta_2)\big) \big\langle (\delta\boldsymbol{\alpha}, \delta\theta), (\delta\boldsymbol{\alpha}, \delta\theta) \big\rangle \\ \leq C \left(\|\boldsymbol{\alpha}_1 - \boldsymbol{\alpha}_2\|_{\mathrm{H}^1(0,s_F)} + \|\theta_1 - \theta_2\|_{\mathrm{H}^1(0,s_F)} \right) \left(\|\delta\boldsymbol{\alpha}\|^2_{\mathrm{H}^1(0,s_F)} + \|\delta\theta\|^2_{\mathrm{H}^1(0,s_F)} \right)\end{aligned}$$

where $\delta\boldsymbol{\alpha} = (\boldsymbol{\alpha} - \bar{\boldsymbol{\alpha}})$, $\delta\theta = (\theta - \bar{\theta})$. We omit the details for brevity. □

3 Discretization

This section is devoted to the numerical approximation of the minimization problems (2.5) and (2.13a). For simplicity, we first introduce a parametrization of the moving domain (D_t and D_s) in terms of a fixed domain $\widehat{D}$. After rewriting the minimization problem in terms of $\widehat{D}$, we will introduce a discrete formulation and prove H^1-weak convergence of its solution to a minimizer of the continuous problem. Such a proof is motivated by Γ-convergence theory [7, 2]. Moreover, for problem (2.13a) we prove the H^1-strong convergence of the discrete problem to a local minimizer of (2.5).

3.1 Problem 1: Fixed final time

Given that the domain D_t changes with time, suitable assumptions are needed in order to define a time discrete approximation of the minimization problem. With this in mind, we define a reference domain $\widehat{D} \subset \mathbb{R}^d$ and a map $\mathbf{X} : [0, T] \times \overline{\widehat{D}} \to \overline{\mathcal{O}}$, such that for all $t \in [0, T]$

$$\begin{aligned}\mathbf{X}(t, \cdot) : \overline{\widehat{D}} &\to \overline{D}_t \\ \widehat{\boldsymbol{x}} &\to \boldsymbol{x} = \mathbf{X}(t, \widehat{\boldsymbol{x}}),\end{aligned}$$

is a one-to-one correspondence which satisfies $\mathbf{X}(t, \widehat{D}) = D_t$. For simplicity, we assume

$$\mathbf{X}(t, \widehat{\boldsymbol{x}}) = \boldsymbol{\varphi}(t) + \psi(t)\widehat{\boldsymbol{x}},$$

where

$$\boldsymbol{\varphi} : [0, T] \to \mathbb{R}^d, \quad \psi : [0, T] \to (0, +\infty), \quad \boldsymbol{\varphi}, \psi \in \mathrm{H}^1(0, T) \tag{3.1}$$

are functions such that $\boldsymbol{\varphi}(0) = \mathbf{0}$ and $\psi(0) = 1$, namely $\widehat{D} = D_0$. In case $\psi(t) = \widehat{\psi} \in \mathbb{R}^+$ for all $t \in [0, T]$, $\boldsymbol{\varphi}$ can be viewed as a parameterization of a desired path that the scaled domain $\widehat{\psi}\widehat{D}$ traverses from an initial position to a final position. However, in applications such as magnetic drug targeting, a general function $\psi(t)$ may be needed to control drug spreading. Therefore, for $i = 1, \ldots, d$

$$\begin{aligned}\int_0^T \int_{D_t} \Big(\boldsymbol{\alpha}(t)^\top \boldsymbol{P}_i(\boldsymbol{x}) \boldsymbol{\alpha}(t) - \mathrm{f}_i(t, \boldsymbol{x}) \Big)^2 \, d\boldsymbol{x} \, dt \\ = \int_0^T \int_{\widehat{D}} \Big(\boldsymbol{\alpha}(t)^\top \boldsymbol{P}_i(\mathbf{X}(t, \widehat{\boldsymbol{x}})) \psi(t)^{d/2} \boldsymbol{\alpha}(t) - \mathrm{f}_i(t, \mathbf{X}(t, \widehat{\boldsymbol{x}})) \psi(t)^{d/2} \Big)^2 \, d\widehat{\boldsymbol{x}} \, dt,\end{aligned}$$

because $\det(\nabla_{\widehat{\boldsymbol{x}}}\mathbf{X}(t,\widehat{\boldsymbol{x}})) = \psi(t)^d$. Then, we rewrite $\mathcal{J}$ as

$$\mathcal{J}(\boldsymbol{\alpha}) = \frac{1}{2}\sum_{i=1}^{d}\int_0^T \|\boldsymbol{\alpha}^\top \widehat{\boldsymbol{P}}_i\boldsymbol{\alpha} - \widehat{\mathrm{f}}_i\|^2_{\mathrm{L}^2(\widehat{D})} + \frac{\lambda}{2}\int_0^T |d_t\boldsymbol{\alpha}|^2 = \mathcal{J}^1(\boldsymbol{\alpha}) + \mathcal{J}^2(\boldsymbol{\alpha}) \tag{3.2}$$

with $\widehat{\boldsymbol{P}}_i(t,\widehat{\boldsymbol{x}}) := \boldsymbol{P}_i(\mathbf{X}(t,\widehat{\boldsymbol{x}}))\psi(t)^{d/2}$ and $\widehat{\mathrm{f}}_i(t,\widehat{\boldsymbol{x}}) = \mathrm{f}_i(t,\mathbf{X}(t,\widehat{\boldsymbol{x}}))\psi(t)^{d/2}$, $i = 1,\dots,d$.

Next, we introduce a time discretization of the Problem 1 upon using $\mathcal{J}$ as defined in (3.2). Let us fix $N \in \mathbb{N}$ and let $\tau := T/N$ be the time step. Now, for $n = 1,\dots,N$, we define $t^n := n\tau$, $\widehat{\boldsymbol{P}}_i^n = \widehat{\boldsymbol{P}}_i(t^n)$ and $\widehat{\mathrm{f}}_i^n$ to be

$$\widehat{\mathrm{f}}_i^n(\cdot) = \frac{1}{\tau}\int_{t^{n-1}}^{t^n} \widehat{\mathrm{f}}_i(t,\cdot)dt, \qquad i = 1,\dots,d, \tag{3.3}$$

which in turn allows us to incorporate a general $\mathbf{f}$. Then we consider a time discrete version of (2.5): given the initial condition $\boldsymbol{\alpha}_0 =: \bar{\boldsymbol{\alpha}}_\tau(0)$ (cf. (2.4)), find $\bar{\boldsymbol{\alpha}}_\tau \in \mathcal{H}^\tau_{ad}$ solving

$$\bar{\boldsymbol{\alpha}}_\tau = \underset{\boldsymbol{\alpha}_\tau \in \mathcal{H}^\tau_{ad}}{\arg\min}\, \mathcal{J}_\tau(\boldsymbol{\alpha}_\tau), \quad \mathcal{J}_\tau(\boldsymbol{\alpha}_\tau) = \mathcal{J}^1_\tau(\boldsymbol{\alpha}_\tau) + \mathcal{J}^2_\tau(\boldsymbol{\alpha}_\tau), \tag{3.4}$$

where

$$\mathcal{J}^1_\tau(\boldsymbol{\alpha}_\tau) = \tau\sum_{n=1}^{N}\frac{1}{2}\sum_{i=1}^{d}\|(\boldsymbol{\alpha}_\tau^n)^\top \widehat{\boldsymbol{P}}_i^n\boldsymbol{\alpha}_\tau^n - \widehat{\mathrm{f}}_i^n\|^2_{\mathrm{L}^2(\widehat{D})}, \quad \mathcal{J}^2_\tau(\boldsymbol{\alpha}_\tau) = \tau\sum_{n=1}^{N}\frac{\lambda}{2\tau^2}|\boldsymbol{\alpha}_\tau^n - \boldsymbol{\alpha}_\tau^{n-1}|^2$$

and

$$\mathcal{H}^\tau_{ad} := \{\boldsymbol{\alpha}_\tau \in \mathrm{H}^1(0,T) : \boldsymbol{\alpha}_\tau|_{[t^{n-1},t^n]} \in \mathbb{P}^1,\ n = 1,\dots,N\} \cap \mathcal{H}_{ad}.$$

Hereafter $\mathbb{P}^1$ is the space of polynomials of degree at most 1. Moreover, by applying the same arguments of Theorem 2.2, it follows that there exists $\bar{\boldsymbol{\alpha}}_\tau \in \mathcal{H}^\tau_{ad}$ solution to problem (3.4).

Notice that $\mathcal{J}$ is a non-convex functional, so convergence of discrete minimizers to a continuous one is not immediate. The convergence of the discrete scheme is the content of the next result which is motivated by Γ-convergence.

Theorem 3.1 (Problem 1: convergence to global minimizers)**.** *The family of global minimizers* $\{\bar{\boldsymbol{\alpha}}_\tau\}_{\tau>0}$ *to* (3.4) *is uniformly bounded in* $\mathrm{H}^1(0,T)$ *and it contains a subsequence that converges weakly to* $\bar{\boldsymbol{\alpha}}$ *in* $\mathrm{H}^1(0,T)$*, a global solution to the minimization problem* (2.5)*, and* $\lim_{\tau\to 0}\mathcal{J}_\tau(\bar{\boldsymbol{\alpha}}_\tau) = \mathcal{J}(\bar{\boldsymbol{\alpha}})$*.*

Proof. We proceed is several steps.

1.- *Boundedness of* $\{\bar{\boldsymbol{\alpha}}_\tau\}_{\tau>0}$ *in* $\mathrm{H}^1(0,T)$*:* This follows immediately from the fact that $\bar{\boldsymbol{\alpha}}_\tau$ minimizes $\mathcal{J}_\tau$ and $\lambda > 0$: given that the constant function $\boldsymbol{\alpha}_0(t) = \boldsymbol{\alpha}_0$ belongs to $\mathcal{H}^\tau_{ad}$, we have

$$\mathcal{J}_\tau(\bar{\boldsymbol{\alpha}}_\tau) \le \mathcal{J}_\tau(\boldsymbol{\alpha}_0) \le C\left(|\boldsymbol{\alpha}_0|^4 + \|\mathbf{f}\|^2_{\mathrm{L}^2(0,T;\mathrm{L}^2(\emptyset))}\right).$$

This implies the existence of a (not relabeled) weakly convergent subsequence such that $\bar{\boldsymbol{\alpha}}_\tau \rightharpoonup \bar{\boldsymbol{\alpha}}$ in $\mathrm{H}^1(0,T)$ and $\bar{\boldsymbol{\alpha}} \in \mathcal{H}_{ad}$. It remains to prove that $\bar{\boldsymbol{\alpha}}$ solves (2.5) and $\lim_{\tau\to 0} \mathcal{J}_\tau(\bar{\boldsymbol{\alpha}}_\tau) = \mathcal{J}(\bar{\boldsymbol{\alpha}})$.

2.- *Lower bound inequality*: We show that

$$\mathcal{J}(\boldsymbol{\alpha}) \leq \liminf_{\tau\to 0} \mathcal{J}_\tau(\boldsymbol{\alpha}_\tau). \tag{3.5}$$

for all $\{\boldsymbol{\alpha}_\tau\}_{\tau>0} \subset \mathcal{H}^\tau_{ad}$ converging to $\boldsymbol{\alpha}$ weakly in $\mathrm{H}^1(0,T)$. Consequently $\boldsymbol{\alpha}_\tau \to \boldsymbol{\alpha}$ in strongly in $\mathrm{L}^2(0,T)$ for a subsequence (not relabeled). If $\overline{\Pi}_\tau \boldsymbol{\alpha}_\tau$ is the piecewise constant interpolant of $\boldsymbol{\alpha}_\tau$, then

$$\|\overline{\Pi}_\tau \boldsymbol{\alpha}_\tau - \boldsymbol{\alpha}\|_{\mathrm{L}^2(0,T)} \leq \|\overline{\Pi}_\tau \boldsymbol{\alpha}_\tau - \boldsymbol{\alpha}_\tau\|_{\mathrm{L}^2(0,T)} + \|\boldsymbol{\alpha}_\tau - \boldsymbol{\alpha}\|_{\mathrm{L}^2(0,T)} \to 0,$$

because $\{d_t \boldsymbol{\alpha}_\tau\}_{\tau>0}$ being bounded implies $\|\overline{\Pi}_\tau \boldsymbol{\alpha}_\tau - \boldsymbol{\alpha}_\tau\|_{\mathrm{L}^2(0,T)} \to 0$. In view of the smoothness of $\widehat{\boldsymbol{P}}_i$, if $\overline{\widehat{\boldsymbol{P}}}_i$ denotes the piecewise constant interpolation in time then $\overline{\widehat{\boldsymbol{P}}}_i \to \widehat{\boldsymbol{P}}_i$ in $\mathrm{L}^2(0,T;\mathrm{L}^2(\widehat{D}))$, $i = 1,\dots,d$. Collecting these results and using that $\|\boldsymbol{\alpha}_\tau\|_{\mathrm{L}^\infty(0,T)} \leq \boldsymbol{\alpha}^*$, we readily obtain

$$\overline{\Pi}_\tau \boldsymbol{\alpha}_\tau^\top \overline{\widehat{\boldsymbol{P}}}_i \overline{\Pi}_\tau \boldsymbol{\alpha}_\tau \to \boldsymbol{\alpha}^\top \widehat{\boldsymbol{P}}_i \boldsymbol{\alpha} \quad \text{in } \mathrm{L}^2(0,T;\mathrm{L}^2(\widehat{D})),$$

which in conjunction with the regularity of $\mathbf{f}$ leads to

$$\mathcal{J}^1_\tau(\boldsymbol{\alpha}_\tau) \to \mathcal{J}^1(\boldsymbol{\alpha}). \tag{3.6}$$

On the other hand, given that $d_t \boldsymbol{\alpha}_\tau$ converges weakly to $d_t \boldsymbol{\alpha}$ in $\mathrm{L}^2(0,T)$, from the weak lower semi-continuity of the semi-norm it follows that

$$\mathcal{J}^2(\boldsymbol{\alpha}) \leq \liminf_{\tau\to 0} \mathcal{J}^2_\tau(\boldsymbol{\alpha}_\tau). \tag{3.7}$$

From (3.6) and (3.7) we conclude

$$\mathcal{J}(\boldsymbol{\alpha}) \leq \liminf_{\tau\to 0} \mathcal{J}^1_\tau(\boldsymbol{\alpha}_\tau) + \liminf_{\tau\to 0} \mathcal{J}^2_\tau(\boldsymbol{\alpha}_\tau) \leq \liminf_{\tau\to 0} \mathcal{J}_\tau(\boldsymbol{\alpha}_\tau).$$

3.- *Existence of a recovery sequence*: Let $\boldsymbol{\alpha} \in \mathcal{H}_{ad}$ be given. Then, the piecewise linear Lagrange interpolant $\Pi_\tau \boldsymbol{\alpha}$ of $\boldsymbol{\alpha}$, belongs to $\mathcal{H}^\tau_{ad}$. Since $d_t(\Pi_\tau \boldsymbol{\alpha}) \to d_t \boldsymbol{\alpha}$ in $\mathrm{L}^2(0,T)$ and $\Pi_\tau \boldsymbol{\alpha}_\tau^\top \overline{\widehat{\boldsymbol{P}}}_i \Pi_\tau \boldsymbol{\alpha}_\tau \to \boldsymbol{\alpha}^\top \widehat{\boldsymbol{P}}_i \boldsymbol{\alpha}$ in $\mathrm{L}^2(0,T;\mathrm{L}^2(\widehat{D}))$ because $\|\Pi_\tau \boldsymbol{\alpha}\|_{\mathrm{L}^\infty(0,T)} \leq \boldsymbol{\alpha}^*$, we obtain

$$\limsup_{\tau\to 0} \mathcal{J}_\tau(\Pi_\tau \boldsymbol{\alpha}) \leq \limsup_{\tau\to 0} \mathcal{J}^1_\tau(\Pi_\tau \boldsymbol{\alpha}) + \limsup_{\tau\to 0} \mathcal{J}^2_\tau(\Pi_\tau \boldsymbol{\alpha}) \leq \mathcal{J}(\boldsymbol{\alpha}).$$

4.- $\bar{\boldsymbol{\alpha}}$ *is a global minimizer for Problem 1:* We need to show

$$\mathcal{J}(\boldsymbol{v}) \geq \mathcal{J}(\bar{\boldsymbol{\alpha}}) \qquad \forall \boldsymbol{v} \in \mathcal{H}_{ad}. \tag{3.8}$$

From step 3 there exists $\{\boldsymbol{v}_\tau\}_{\tau>0}$ such that $\boldsymbol{v}_\tau \rightharpoonup \boldsymbol{v}$ in $\mathrm{H}^1(0,T)$ and

$$\mathcal{J}(\boldsymbol{v}) \geq \limsup_{\tau\to 0} \mathcal{J}_\tau(\boldsymbol{v}_\tau) \geq \liminf_{\tau\to 0} \mathcal{J}_\tau(\boldsymbol{v}_\tau) \geq \liminf_{\tau\to 0} \mathcal{J}_\tau(\bar{\boldsymbol{\alpha}}_\tau) \geq \mathcal{J}(\bar{\boldsymbol{\alpha}})$$

where we have used that $\bar{\boldsymbol{\alpha}}_\tau$ is a global minimizer for $\mathcal{J}_\tau$ together with (3.5).

5.- *Convergence:* Since $\bar{\boldsymbol{\alpha}}_\tau$ is a global minimizer we deduce $\mathcal{J}_\tau(\bar{\boldsymbol{\alpha}}_\tau) \leq \mathcal{J}_\tau(\Pi_\tau \bar{\boldsymbol{\alpha}})$, whence applying first step 3 and next step 2 we see that

$$\limsup_{\tau\to 0} \mathcal{J}_\tau(\bar{\boldsymbol{\alpha}}_\tau) \leq \limsup_{\tau\to 0} \mathcal{J}_\tau(\Pi_\tau \bar{\boldsymbol{\alpha}}) \leq \mathcal{J}(\bar{\boldsymbol{\alpha}}) \leq \liminf_{\tau\to 0} \mathcal{J}_\tau(\bar{\boldsymbol{\alpha}}_\tau).$$

This implies $\lim_{\tau\to 0} \mathcal{J}_\tau(\bar{\boldsymbol{\alpha}}_\tau) = \mathcal{J}(\bar{\boldsymbol{\alpha}})$. In addition $\{\bar{\boldsymbol{\alpha}}_\tau\}_{\tau>0}$ converges L^2-strongly and H^1-weakly to $\bar{\boldsymbol{\alpha}}$, a global minimizer of (2.5).

This concludes the proof. □

Remark 3.2 (quadrature)**.** In general, numerical integration has to be used to compute the space integrals in (3.4), leading to another approximation error. For simplicity, we have assumed that we can evaluate the integrals exactly.

Given that $\mathcal{J}$ is non-convex, the solution to (2.5) might not be unique. However, the minimizers are locally unique if we assume the second-order optimality condition (2.8) (cf. Lemma 2.4). We also notice that the previous convergence result, Theorem 3.1, does not guarantee the convergence to one of these local minimizers but to a global one. To rectify this we follow [5]. Let us first assume that $\bar{\boldsymbol{\alpha}}$ is a local unique solution to (2.3a). For a fixed $\varepsilon > 0$, we construct a family $\{\boldsymbol{\alpha}_\tau^\varepsilon\}_{\tau>0}$ upon solving the minimization problem

$$\boldsymbol{\alpha}_\tau^\varepsilon = \operatorname*{arg\,min}_{\boldsymbol{\alpha}_\tau \in \mathcal{H}_{ad}^{\tau,\varepsilon}} \mathcal{J}_\tau(\boldsymbol{\alpha}_\tau) \tag{3.9}$$

in an $\varepsilon-$neighborhood of $\bar{\boldsymbol{\alpha}}$ denoted by $\mathcal{H}_{ad}^{\tau,\varepsilon} = \Big\{\boldsymbol{\alpha}_\tau \in \mathcal{H}_{ad}^\tau : \|\Pi_\tau \bar{\boldsymbol{\alpha}} - \boldsymbol{\alpha}_\tau\|_{\mathrm{L}^2(0,T)} \leq \varepsilon\Big\}$.

Next, we prove that $\{\boldsymbol{\alpha}_\tau^\varepsilon\}_{\tau>0}$ forms the local solution to the problem (3.4). First, we recall the definition of ν from (2.9) and define $\bar{\varepsilon} := \dfrac{\nu}{2}$. It follows from the definition of Π_τ that there exist a $\tau_0 > 0$ such that for every $\tau \leq \tau_0$ we have $\|\Pi_\tau \bar{\boldsymbol{\alpha}} - \bar{\boldsymbol{\alpha}}\|_{\mathrm{L}^2(0,T)} \leq \dfrac{\nu}{2}$. Then, for a given $\boldsymbol{\alpha} \in \mathcal{H}_{ad}^{\tau,\varepsilon}$, $\varepsilon \leq \bar{\varepsilon}$, and $\tau \leq \tau_0$ we obtain

$$\|\boldsymbol{\alpha} - \bar{\boldsymbol{\alpha}}\|_{\mathrm{L}^2(0,T)} \leq \|\Pi_\tau \bar{\boldsymbol{\alpha}} - \boldsymbol{\alpha}\|_{\mathrm{L}^2(0,T)} + \|\Pi_\tau \bar{\boldsymbol{\alpha}} - \bar{\boldsymbol{\alpha}}\|_{\mathrm{L}^2(0,T)} \leq \nu.$$

Finally, in view of (2.9) we arrive at

$$\mathcal{J}(\boldsymbol{\alpha}) \geq \mathcal{J}(\bar{\boldsymbol{\alpha}}) + \hat{C}\|\boldsymbol{\alpha} - \bar{\boldsymbol{\alpha}}\|^2_{\mathrm{H}^1(0,T)} \qquad \forall \boldsymbol{\alpha} \in \mathcal{H}_{ad}^{\tau,\varepsilon}. \tag{3.10}$$

Such a quadratic behavior enables us to prove the following convergence result for the family $\{\boldsymbol{\alpha}_\tau^\varepsilon\}_{\tau>0}$ solving (3.9).

Lemma 3.3 (Problem 1: convergence to local minimizers)**.** *Let $\bar{\boldsymbol{\alpha}} \in \mathcal{H}_{ad}$ be a local unique minimizer of* (2.3)*. If $\varepsilon \leq \bar{\varepsilon}$ and $\{\boldsymbol{\alpha}_\tau^\varepsilon\}_{\tau>0}$ solves* (3.9)*, then there exists a $\tau_0 > 0$ such that for all $\tau \leq \tau_0$, $\mathcal{J}_\tau(\boldsymbol{\alpha}_\tau^\varepsilon) \to \mathcal{J}(\bar{\boldsymbol{\alpha}})$ and $\|\boldsymbol{\alpha}_\tau^\varepsilon - \bar{\boldsymbol{\alpha}}\|_{\mathrm{H}^1(0,T)} \to 0$ as $\tau \to 0$. Moreover, $\boldsymbol{\alpha}_\tau^\varepsilon$ is a local solution of* (3.4)*, i.e*

$$\mathcal{J}_\tau(\boldsymbol{\alpha}_\tau^\varepsilon) \leq \mathcal{J}_\tau(\boldsymbol{\alpha}_\tau) \tag{3.11}$$

for all $\boldsymbol{\alpha}_\tau \in \mathcal{H}_{ad}^\tau$ such that $\|\boldsymbol{\alpha}_\tau^\varepsilon - \boldsymbol{\alpha}_\tau\|_{\mathrm{L}^2(0,T)} \leq \varepsilon/2$.

Proof. Notice that, because of the regularity assumption (3.1) on $\boldsymbol{\varphi}$ and ψ, it is straightforward to prove that

$$\begin{aligned} |\mathcal{J}_\tau(\boldsymbol{\alpha}_\tau) - \mathcal{J}(\boldsymbol{\alpha}_\tau)| \to 0 \qquad & \forall \boldsymbol{\alpha}_\tau \in \mathcal{H}_{ad}^\tau, \\ \mathcal{J}(\Pi_\tau \boldsymbol{\alpha}) \to \mathcal{J}(\boldsymbol{\alpha}) \qquad & \forall \boldsymbol{\alpha} \in \mathcal{H}_{ad}. \end{aligned} \tag{3.12}$$

On the other hand, from (3.10) we obtain

$$\begin{aligned} \mathcal{J}_\tau(\boldsymbol{\alpha}_\tau^\varepsilon) &\geq \mathcal{J}(\bar{\boldsymbol{\alpha}}) + (\mathcal{J}_\tau(\boldsymbol{\alpha}_\tau^\varepsilon) - \mathcal{J}(\boldsymbol{\alpha}_\tau^\varepsilon)) + \hat{C}\|\boldsymbol{\alpha}_\tau^\varepsilon - \bar{\boldsymbol{\alpha}}\|^2_{\mathrm{H}^1(0,T)} \\ &\geq \mathcal{J}(\bar{\boldsymbol{\alpha}}) - |\mathcal{J}_\tau(\boldsymbol{\alpha}_\tau^\varepsilon) - \mathcal{J}(\boldsymbol{\alpha}_\tau^\varepsilon)|. \end{aligned} \tag{3.13}$$

Moreover, given that $\Pi_\tau \bar{\boldsymbol{\alpha}} \in \mathcal{H}_{ad}^{\tau,\varepsilon}$, from the optimality of $\boldsymbol{\alpha}_\tau^\varepsilon$ it follows that

$$\mathcal{J}_\tau(\boldsymbol{\alpha}_\tau^\varepsilon) \leq \mathcal{J}_\tau(\Pi_\tau \bar{\boldsymbol{\alpha}}) = \mathcal{J}(\bar{\boldsymbol{\alpha}}) + \big(\mathcal{J}_\tau(\Pi_\tau \bar{\boldsymbol{\alpha}}) - \mathcal{J}(\Pi_\tau \bar{\boldsymbol{\alpha}})\big) + \big(\mathcal{J}(\Pi_\tau \bar{\boldsymbol{\alpha}}) - \mathcal{J}(\bar{\boldsymbol{\alpha}})\big). \tag{3.14}$$

Then, from (3.12)-(3.14) we obtain

$$\mathcal{J}_\tau(\boldsymbol{\alpha}_\tau^\varepsilon) \to \mathcal{J}(\bar{\boldsymbol{\alpha}}), \tag{3.15}$$

which is the first assertion. The second assertion $\|\boldsymbol{\alpha}_\tau^\varepsilon - \bar{\boldsymbol{\alpha}}\|^2_{\mathrm{H}^1(0,T)} \to 0$ is now a trivial consequence of the middle inequality in (3.13) together with (3.12) and (3.15). It remains to show (3.11). Let $\boldsymbol{\alpha}_\tau \in \mathcal{H}_{ad}^\tau$ satisfy $\|\boldsymbol{\alpha}_\tau - \boldsymbol{\alpha}_\tau^\varepsilon\|_{\mathrm{L}^2(0,T)} \leq \dfrac{\varepsilon}{2}$. Then for τ small enough we arrive at

$$\|\boldsymbol{\alpha}_\tau - \Pi_\tau \bar{\boldsymbol{\alpha}}\|_{\mathrm{L}^2(0,T)} \leq \|\boldsymbol{\alpha}_\tau - \boldsymbol{\alpha}_\tau^\varepsilon\|_{\mathrm{L}^2(0,T)} + \|\bar{\boldsymbol{\alpha}} - \boldsymbol{\alpha}_\tau^\varepsilon\|_{\mathrm{L}^2(0,T)} + \|\Pi_\tau \bar{\boldsymbol{\alpha}} - \bar{\boldsymbol{\alpha}}\|_{\mathrm{L}^2(0,T)} \leq \varepsilon.$$

Thus, $\boldsymbol{\alpha}_\tau$ belongs to $\mathcal{H}_{ad}^{\tau,\varepsilon}$ and (3.11) follows from (3.9). □

3.2 Problem 2: Minimizing the final time

Like in Section 3.1, in order to handle the first term in (2.13b), we consider a parametrization of the moving domain D_s but now defined in terms of the arc length s, namely

$$\mathbf{X}(s, \widehat{\boldsymbol{x}}) = \boldsymbol{\rho}(s) + \widetilde{\psi}(s)\widehat{\boldsymbol{x}} \qquad \forall \widehat{\boldsymbol{x}} \in \widehat{D}, \quad 0 \leq s \leq s_F,$$

where $\widetilde{\psi}$ belongs to $\mathrm{H}^1(0, s_F)$ and $\boldsymbol{\rho} \in C^1[0, s_F]$. Then, the functional $\mathcal{F}$ in (2.13b) reduces to

$$\mathcal{F}(\boldsymbol{\alpha}, \theta) = \mathcal{F}^1(\boldsymbol{\alpha}, \theta) + \mathcal{F}^2(\theta) + \mathcal{F}^3(\alpha) + \mathcal{F}^4(\theta)$$

with

$$\mathcal{F}^1(\boldsymbol{\alpha}, \theta) = \int_0^{s_F} \frac{1}{2\theta(s)} \sum_{i=1}^{d} \|\boldsymbol{\alpha}(s)^\top \widetilde{\boldsymbol{P}}_i \boldsymbol{\alpha}(s) - \boldsymbol{\rho}_i'(s)\widetilde{\theta}(s)\|^2_{\mathrm{L}^2(\widehat{D})} ds,$$

$$\mathcal{F}^2(\theta) = \int_0^{s_F} \frac{\beta}{\theta(s)} ds, \quad \mathcal{F}^3(\boldsymbol{\alpha}) = \int_0^{s_F} \frac{\lambda}{2} |d_s \boldsymbol{\alpha}(s)|^2 ds, \quad \mathcal{F}^4(\theta) = \int_0^{s_F} \frac{\eta}{2} |d_s \theta(s)|^2 ds$$

and $\widetilde{\boldsymbol{P}}_i(\widehat{\boldsymbol{x}},s) = \boldsymbol{P}_i(\mathbf{X}(s,\widehat{\boldsymbol{x}}))\widetilde{\psi}^{d/2}(s)$, $i=1,\dots,d$, $\widetilde{\theta}(s) = \theta(s)\widetilde{\psi}^{d/2}(s)$. Notice that now the L^2-norm in $\mathcal{F}^1$ is computed on $\widehat{D}$ instead of D_s. Then we introduce a space discretization of (2.13b) by taking into account the previous definition of $\mathcal{F}$. Let us fix $M \in \mathbb{N}$ and set $\kappa := s_F/M$. Now, for $m = 1,\dots,M$, we define $s^m := m\kappa$, $\boldsymbol{\alpha}^m := \boldsymbol{\alpha}(s^m)$, $\theta^m := \theta(s^m)$, $\widetilde{\theta}^m := \widetilde{\theta}(s^m)$, and $\widetilde{\boldsymbol{P}}_i^m = \widetilde{\boldsymbol{P}}_i(s^m)$, $i=1,\dots,d$. Then we consider the following discrete problem: given an initial condition $(\boldsymbol{\alpha}_0,\theta_0) =: (\boldsymbol{\alpha}_\kappa(0),\theta_\kappa(0))$ find a solution $(\boldsymbol{\alpha}_\kappa,\theta_\kappa) \in \mathcal{U}_{ad}^\kappa \times \mathcal{V}_{ad}^\kappa$ to

$$\min_{(\boldsymbol{\alpha}_\kappa,\theta_\kappa)\in\mathcal{U}_{ad}^\kappa\times\mathcal{V}_{ad}^\kappa} \mathcal{F}_\kappa(\boldsymbol{\alpha}_\kappa,\theta_\kappa), \quad \mathcal{F}_\kappa(\boldsymbol{\alpha}_\kappa,\theta_\kappa) = \mathcal{F}_\kappa^1(\boldsymbol{\alpha}_\kappa,\theta_\kappa) + \mathcal{F}_\kappa^2(\theta_\kappa) + \mathcal{F}_\kappa^3(\boldsymbol{\alpha}_\kappa) + \mathcal{F}_\kappa^4(\theta_\kappa) \tag{3.16}$$

where

$$\mathcal{F}_\kappa^1(\boldsymbol{\alpha}_\kappa,\theta_\kappa) = \sum_{m=1}^M \frac{\kappa}{2\theta_\kappa^m} \sum_{i=1}^d \|(\boldsymbol{\alpha}_\kappa^m)^\top \widetilde{\boldsymbol{P}}_i^m \boldsymbol{\alpha}_\kappa^m - \boldsymbol{\rho}_i'(s^m)\widetilde{\theta}_\kappa^m\|^2_{\mathrm{L}^2(\widehat{D})}, \quad \mathcal{F}_\kappa^2(\theta_\kappa) = \sum_{m=1}^M \frac{\beta\kappa}{\theta_\kappa^m},$$
$$\mathcal{F}_\kappa^3(\boldsymbol{\alpha}_\kappa) = \kappa \sum_{m=1}^M \frac{\lambda}{2\kappa^2}|\boldsymbol{\alpha}_\kappa^m - \boldsymbol{\alpha}_\kappa^{m-1}|^2, \quad \mathcal{F}_\kappa^4(\theta_\kappa) = \kappa \sum_{m=1}^M \frac{\eta}{2\kappa^2}|\theta_\kappa^m - \theta_\kappa^{m-1}|^2,$$

and admissible sets

$$\mathcal{U}_{ad}^\kappa := \left\{\boldsymbol{\alpha}_\kappa \in \mathrm{H}^1(0,s_F) : \boldsymbol{\alpha}_\kappa|_{[s^{m-1},s^m]} \in \mathbb{P}^1, m=1,\dots,M\right\} \cap \mathcal{U}_{ad},$$
$$\mathcal{V}_{ad}^\kappa := \left\{\theta_\kappa \in \mathrm{H}^1(0,s_F) : \theta_\kappa|_{[s^{m-1},s^m]} \in \mathbb{P}^1, m=1,\dots,M\right\} \cap \mathcal{V}_{ad}.$$

Since (3.16) is a finite dimensional problem, the box constrains and the continuity of $\mathcal{F}_\kappa$ implies the existence of a solution $\left(\bar{\boldsymbol{\alpha}}_\kappa,\bar{\theta}_\kappa\right)$ to (3.16).

Theorem 3.4 (Problem 2: convergence to global minimizers)**.** *The family of global minimizers* $\left\{\left(\bar{\boldsymbol{\alpha}}_\kappa,\bar{\theta}_\kappa\right)\right\}_{\kappa>0}$ *to* (3.16) *is uniformly bounded and it contains a subsequence that converges* $\mathrm{H}^1(0,s_F)$*-weak to* $\left(\bar{\boldsymbol{\alpha}},\bar{\theta}\right)$*, a global minimizer of* (2.13a)*, and* $\lim_{\kappa\to0}\mathcal{F}_\kappa(\bar{\boldsymbol{\alpha}}_\kappa,\bar{\theta}_\kappa) = \mathcal{F}(\bar{\boldsymbol{\alpha}},\bar{\theta})$*.*

Proof. As in Theorem 3.1 we proceed in several steps.

1.- *Boundedness of* $\left\{(\bar{\boldsymbol{\alpha}}_\kappa,\bar{\theta}_\kappa)\right\}_\kappa$ *in* $[\mathrm{H}^1(0,s_F)]^2$: Given that the constant function $\left(\boldsymbol{\alpha}_0(s),\theta_0(s)\right) = (\boldsymbol{\alpha}_0,\theta_0)$ belongs to $\mathcal{U}_{ad}^\kappa \times \mathcal{V}_{ad}^\kappa$ and the fact that $\left(\bar{\boldsymbol{\alpha}}_\kappa,\bar{\theta}_\kappa\right)$ minimizes $\mathcal{F}_\kappa$ we have the bound

$$\mathcal{F}_\kappa(\bar{\boldsymbol{\alpha}}_\kappa,\bar{\theta}_\kappa) \le \mathcal{F}_\kappa(\boldsymbol{\alpha}_0,\theta_0) \le C\left(\frac{|\boldsymbol{\alpha}_0|^4}{|\theta_0|} + |\theta_0| + \frac{1}{|\theta_0|}\right).$$

Since $\lambda,\eta>0$, this implies a uniform bound for $(\bar{\boldsymbol{\alpha}}_\kappa,\bar{\theta}_\kappa)$ in $\mathrm{H}^1(0,s_F)$ and the existence of a (not relabeled) subsequence that converge to $(\bar{\boldsymbol{\alpha}},\bar{\theta})$ weakly in $[\mathrm{H}^1(0,s_F)]^2$ and strongly in $[C([0,s_F])]^2$.

2.- *Lower bound inequality*: Let us consider a sequence $\{(\boldsymbol{\alpha}_\kappa,\theta_\kappa)\}_{\kappa>0}\subset \mathcal{U}_{ad}^\kappa\times\mathcal{V}_{ad}^\kappa$ that converges weakly to $(\boldsymbol{\alpha},\theta)$ in $[\mathrm{H}^1(0,s_F)]^2$. Let $\overline{\Pi}_\kappa$ be the piecewise constant interpolation operator at the nodes $\{s^m\}_{m>0}$. Then by straightforward computations it follows that

$$\|\overline{\Pi}_\kappa\boldsymbol{\alpha}_\kappa-\boldsymbol{\alpha}\|_{\mathrm{L}^2(0,s_f)}\to 0\quad\text{and}\quad\|\overline{\Pi}_\kappa\theta_\kappa-\theta\|_{\mathrm{L}^2(0,s_f)}\to 0.$$

Moreover, from the smoothness of $\widetilde{\boldsymbol{P}}_i$ and $\boldsymbol{\rho}'$, if $\overline{\widetilde{\boldsymbol{P}}}_i$, $\overline{\boldsymbol{\rho}'}$ denote the piecewise constant interpolation in time then $\overline{\boldsymbol{\rho}'}\to\boldsymbol{\rho}'$ and $\overline{\widetilde{\boldsymbol{P}}}_i\to\widetilde{\boldsymbol{P}}_i$ in $\mathrm{L}^2(0,s_f;\mathrm{L}^2(\widehat{D}))$, for $i=1,\dots,r$. This, together with the box constrains of $(\bar{\boldsymbol{\alpha}}_\kappa,\bar\theta_\kappa)$, leads to

$$\begin{aligned}\frac{\overline{\Pi}_\kappa\boldsymbol{\alpha}_\kappa^\top\overline{\widetilde{\boldsymbol{P}}}_i\overline{\Pi}_\kappa\boldsymbol{\alpha}_\kappa}{\overline{\Pi}_\kappa\theta_\kappa^{1/2}}-\overline{\Pi}_\kappa\widetilde{\theta}_\kappa^{1/2}\overline{\boldsymbol{\rho}'}&\to\frac{\boldsymbol{\alpha}^\top\widetilde{\boldsymbol{P}}_i\boldsymbol{\alpha}}{\theta^{1/2}}-\widetilde{\theta}^{1/2}\boldsymbol{\rho}'\quad\text{in }\mathrm{L}^2(0,s_f;\mathrm{L}^2(\widehat{D}))\\ \frac{1}{\overline{\overline{\Pi}_\kappa\theta_\kappa}}&\to\frac{1}{\theta}\quad\text{in }\mathrm{L}^2(0,s_f),\end{aligned}\tag{3.17}$$

which imply

$$\mathcal{F}^1(\boldsymbol{\alpha},\theta)=\lim_{\kappa\to0}\mathcal{F}^1_\kappa(\boldsymbol{\alpha}_\kappa,\theta_\kappa)\quad\text{and}\quad\mathcal{F}^2(\theta)=\lim_{\kappa\to0}\mathcal{F}^2_\kappa(\theta_\kappa).\tag{3.18}$$

On the other hand, given that $d_s\boldsymbol{\alpha}_\kappa$ and $d_s\theta_\kappa$ converge weakly to $d_s\theta$ in $\mathrm{L}^2(0,s_F)$ and $d_s\boldsymbol{\alpha}$, respectively, and $\mathcal{F}^3(\boldsymbol{\alpha}_\kappa)=\mathcal{F}^3_\kappa(\boldsymbol{\alpha}_\kappa)$, $\mathcal{F}^4(\boldsymbol{\alpha}_\kappa)=\mathcal{F}^4_\kappa(\boldsymbol{\alpha}_\kappa)$, invoking the weak lower semi-continuity of the $\mathrm{H}^1(0,T)$ semi-norm we obtain

$$\mathcal{F}^3(\boldsymbol{\alpha})\le\liminf_{\kappa\to0}\mathcal{F}^3_\kappa(\boldsymbol{\alpha}_\kappa)\quad\text{and}\quad\mathcal{F}^4(\theta)\le\liminf_{\kappa\to0}\mathcal{F}^4_\kappa(\theta_\kappa).\tag{3.19}$$

Therefore, from (3.18)-(3.19) we conclude that

$$\begin{aligned}\mathcal{F}(\boldsymbol{\alpha},\theta)&\le\liminf_{\kappa\to0}\mathcal{F}^1_\kappa(\boldsymbol{\alpha}_\kappa,\theta_\kappa)+\liminf_{\kappa\to0}\mathcal{F}^2_\kappa(\theta_\kappa)\\&\quad+\liminf_{\kappa\to0}\mathcal{F}^3_\kappa(\boldsymbol{\alpha}_\kappa)+\liminf_{\kappa\to0}\mathcal{F}^4_\kappa(\theta_\kappa)\le\liminf_{\kappa\to0}\mathcal{F}_\kappa(\boldsymbol{\alpha}_\kappa,\theta_\kappa).\end{aligned}$$

3.- *Existence of a recovery sequence*: If $(\boldsymbol{\alpha},\theta)\in\mathcal{U}_{ad}\times\mathcal{V}_{ad}$, is given, then $(\Pi_\kappa\boldsymbol{\alpha},\Pi_\kappa\theta)$ belongs to $\mathcal{U}_{ad}^\kappa\times\mathcal{V}_{ad}^\kappa$ where Π_κ is the piecewise linear Lagrange interpolation operator. Since $\partial_s(\Pi_\kappa\boldsymbol{\alpha})\to\partial_s\boldsymbol{\alpha}$ in $\mathrm{L}^2(0,s_F)$, $\partial_s(\Pi_\kappa\theta)\to\partial_s\theta$ in $\mathrm{L}^2(0,s_F)$, we proceed as in Step 2 to obtain the convergence of $\mathcal{F}^1_\kappa$ and $\mathcal{F}^2_\kappa$, whence

$$\begin{aligned}\limsup_{\kappa\to0}\mathcal{F}_\kappa(\Pi_\kappa\boldsymbol{\alpha},\Pi_\kappa\theta)&\le\limsup_{\kappa\to0}\mathcal{F}^1_\kappa(\Pi_\kappa\boldsymbol{\alpha},\Pi_\kappa\theta)+\limsup_{\kappa\to0}\mathcal{F}^2_\kappa(\Pi_\kappa\theta)\\&\quad+\limsup_{\kappa\to0}\mathcal{F}^3_\kappa(\Pi_\kappa\boldsymbol{\alpha})+\limsup_{\kappa\to0}\mathcal{F}^4_\kappa(\Pi_\kappa\theta)\le\mathcal{F}(\boldsymbol{\alpha},\theta).\end{aligned}$$

We finally argue as in steps 4 and 5 of Theorem 3.1 to conclude that $(\bar{\boldsymbol{\alpha}},\bar\theta)$ is a global minimizer of (2.13), i.e.

$$\mathcal{F}(\boldsymbol{\alpha},\theta)\ge\mathcal{F}(\bar{\boldsymbol{\alpha}},\bar\theta)\quad\forall(\boldsymbol{\alpha},\theta)\in\mathcal{U}_{ad}\times\mathcal{V}_{ad},$$

$\lim_{\kappa\to0}\mathcal{F}_\kappa(\bar{\boldsymbol{\alpha}}_\kappa,\bar\theta_\kappa)=\mathcal{F}(\bar{\boldsymbol{\alpha}},\bar\theta)$ and $\{\bar{\boldsymbol{\alpha}}_\kappa,\bar\theta_\kappa\}_{\kappa>0}$ converges L^2-strongly and H^1-weakly to $(\bar{\boldsymbol{\alpha}},\bar\theta)$. We skip details for brevity. □

4 Numerical examples

Let us illustrate the performance of the proposed discrete schemes (3.4) and (3.16). For the first scheme we consider the approximation of a constant and time dependent vector field $\mathbf{f}$ (space independent) on D_t. For the second scheme we compute the optimal time and force by solving (3.16). Finally, we use the computed optimal force as an input to an advection-diffusion partial differential equation used in magnetic drug targeting (see [13]). For all examples $\Omega \subset \mathbb{R}^2$ is a ball of unit radius centered at $(0,0)$ and, the dipoles positions and directions are $\boldsymbol{x}_{k+1} = 1.2(\cos(k\pi/4), \sin(k\pi/4))$ and $\widehat{\boldsymbol{d}}_{k+1} = (\cos(k\pi/4), \sin(k\pi/4)), k = 0, \ldots, 7$ ($n_p = 8$), respectively (see Figure 5 (left)).

To solve the minimization problem, we use a MATLAB implementation of the projected BFGS with Armijo line search [18]; alternative strategies such as semi-smooth Newton [14] can be immediately applied as well. The minimization algorithm is terminated when the l^2-norm of the projected gradient is less or equal to 10^{-5}. Besides the initial condition $\boldsymbol{\alpha}_0 \in \mathbb{R}^{n_p}$, the minimization algorithm requires an initial guess for the solution $\bar{\boldsymbol{\alpha}}$. We propose below Algorithm 1 in order to compute an initial guess $\boldsymbol{\alpha}_{int} \in \mathcal{H}^{\tau}_{ad}$. Notice that the speed of convergence of the minimization algorithm is sensitive to the choice of $\boldsymbol{\alpha}_{int}$.

Given $\boldsymbol{\alpha}_*$ and $\boldsymbol{\alpha}^*$, by $\mathrm{Proj}_{[\boldsymbol{\alpha}_*, \boldsymbol{\alpha}^*]}$ we denote pointwise projection on the interval $[\boldsymbol{\alpha}_*, \boldsymbol{\alpha}^*]$

$$\mathrm{Proj}_{[\boldsymbol{\alpha}_*, \boldsymbol{\alpha}^*]}(\mathbf{x}) = \min\left\{\boldsymbol{\alpha}^*, \max\left\{\mathbf{x}, \boldsymbol{\alpha}_*\right\}\right\},$$

where min and max are interpreted componentwise. The aim of Algorithm 1 is to initialize the actual minimization algorithm used to solve (3.4). Notice that the algorithm above is the so-called finite horizon model predictive or instantaneous optimization algorithm [1, 15]: the minimization takes place over one time step only. Under the assumption that solving a one step problem is cheaper, the previous algorithm provides us a "fast" yet "accurate" initial guess to solve (3.4).

Remark 4.1 (non-convexity)**.** Due to the non-convexity of the cost functional $\mathcal{J}$ (and $\mathcal{J}_\tau$), we may converge to different local minima depending on the choice of the initial guess.

Algorithm 1 : Initialization algorithm

1: **Input:** $\boldsymbol{\alpha}_0$, $\boldsymbol{\alpha}_*$, $\boldsymbol{\alpha}^*$, λ, τ, $\widehat{D}$, `tol`, $\widehat{\boldsymbol{P}}_i^n$, $\widehat{\mathrm{f}}_i^n$, $n = 1, \ldots, N$,
2: Set $\mathbf{x}^0 := \boldsymbol{\alpha}_0$
3: **for** $n = 1, \ldots, N$ **do**
4: Solve for $\mathbf{x} \in \mathbb{R}^{n_p}$

$$\min_{\substack{\mathbf{x}\in\mathbb{R}^{n_p} \\ \boldsymbol{\alpha}_* \le \mathbf{x} \le \boldsymbol{\alpha}^*}} J(\mathbf{x}), \qquad J(\mathbf{x}) = \frac{1}{2}\sum_{i=1}^{d} \|\mathbf{x}^\top \widehat{\boldsymbol{P}}_i^n \mathbf{x} - \widehat{\mathrm{f}}_i^n\|^2_{\mathrm{L}^2(\widehat{D})} + \frac{\lambda}{2\tau^2}|\mathbf{x} - \mathbf{x}^0|^2$$

with termination criterion: $|\mathbf{x} - \mathrm{Proj}_{[\boldsymbol{\alpha}_*, \boldsymbol{\alpha}^*]}(\mathbf{x} - \nabla J(\mathbf{x}))| < \mathtt{tol}$.
5: $\boldsymbol{\alpha}_{int}(n\tau) = \mathbf{x}$
6: $\mathbf{x}^0 \leftarrow \mathbf{x}$
7: **end for**

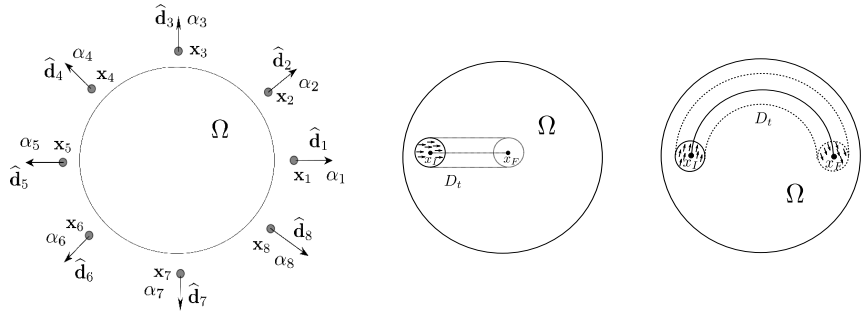


Figure 5: Computational configuration (left) and two different moving subdomains D_t within $\emptyset \subset \mathbb{R}^2$. These domains, $D_{1,t}$ (left) and $D_{2,t}$ (right), do not deform, are initialized at $\boldsymbol{x}_I$ and travel to their destinations $\boldsymbol{x}_F$ along different curves. The target vector fields $\{\mathbf{f}_i\}_{i=1}^2$, which are tangent to the curve $\mathcal{C}$, are represented by arrows for the initial configuration (left) and also for the final configuration (right).

4.1 Problem 1: Approximation of a vector field

We consider the discrete minimization problem (3.4) for two different choices of $\mathbf{f}$ and D_t. The admissible set is characterized by upper and lower bounds $\boldsymbol{\alpha}^* = (2, \ldots, 2) \in \mathbb{R}^8$ and $\boldsymbol{\alpha}_* = (-2, \ldots, -2) \in \mathbb{R}^8$, respectively. The final time is $T = 1$ and the reference domain $\widehat{D}$ is a ball of radius 0.2 centered at $(-0.75, 0)$. We are interested in the approximations of a constant vector field $\mathbf{f}_1(\boldsymbol{x}, t) = (1, 0)^\top$ and a time dependent vector field given by $\mathbf{f}_2(\boldsymbol{x}, t) = (\sin(\pi(1-t)), -\cos(\pi(1-t))^\top$. The moving domains $D_{i,t}$ are such that $D_{i,t} = \boldsymbol{x}_I(t, \widehat{D})$, with $\boldsymbol{x}_I(t, \widehat{\boldsymbol{x}}) = \boldsymbol{\varphi}_i(t) + \widehat{\boldsymbol{x}}$, $i = 1, 2$.

Here $\boldsymbol{\varphi}_1(t) = (t, 0)^\top$ and $\boldsymbol{\varphi}_2(t) = 0.6(\cos(\pi(1-t)), \sin(\pi(1-t))^\top$ represent trajectories of the barycenters of $D_{1,t}$ and $D_{2,t}$, respectively as shown in Figure 5 (center and right). For each of these configurations we have solved problem (3.4) for $N = 80$ time intervals, $\lambda = 10^{-5}$ and initial condition $\boldsymbol{\alpha}_0 = (1, \ldots, 1)^\top \in \mathbb{R}^{n_p}$.

To analyze the discrete optimization problem we consider the approximation of $\mathbf{f}_1$ on $D_{1,t}$ for two initial guesses: constant function $\boldsymbol{\alpha}_{int}^a = \mathbf{1}$ and $\boldsymbol{\alpha}_{int}^b$ given by Algorithm 1 with $\texttt{tol} = 10^{-3}$. Figure 6 (left) shows the initial guess $\boldsymbol{\alpha}_{int}^b$ obtained by Algorithm 1 with a total of 201 iterations. We recall that, at each time step n, the iterations of the minimization problem in Algorithm 1 depends on n_p unknowns. The solution $\bar{\boldsymbol{\alpha}}(t) = (\bar{\alpha}_i(t))_{i=1}^8$ of problem (3.4) with initial guesses given by $\boldsymbol{\alpha}_{int}^b$ and $\boldsymbol{\alpha}_{int}^a$ are depicted in Figure 6 (right) and Figure 7 (left), respectively. We notice that dipoles on the left (dipoles 4, 5 and 6) have small intensities at initial times. Such a behavior is expected because $D_{1,t}$ is close to the boundary of Ω, where the magnetic field generated by these dipoles is large, thus it is difficult for dipoles 4, 5 and 6 to "push" in the $\mathbf{f}_1$ direction. On the other hand, dipoles on the right (dipoles 1, 2 and 8) which can create an attractive field in the $\mathbf{f}_1$ direction, have the largest intensities at initial times.

Figure 7 (right) shows $\mathcal{J}_\tau$ per optimization iteration (log scale). Notice that the number of unknowns at each iteration to solve (3.4) is Nn_p . The minimization algorithm

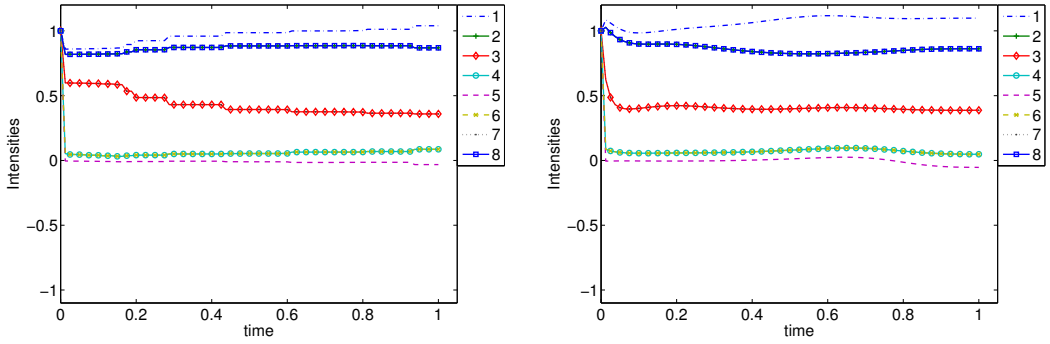


Figure 6: Initial guess $\boldsymbol{\alpha}_{int}^b$ computed by Algorithm 1 (left) and optimal solution $\bar{\boldsymbol{\alpha}}_\tau = (\bar{\alpha}_{i,\tau})_{i=1}^8$ to problem (3.4) with initial guess $\boldsymbol{\alpha}_{int}^b$ (right). The evolution of the intensities is shown for each dipole $i = 1, \ldots, 8$.

to solve (3.4) with initial guess $\boldsymbol{\alpha}_{int}^b$ stops after 3440 iterations, whereas for the initial guess $\boldsymbol{\alpha}_{int}^a$ the stopping criteria is satisfied after 38427 iterations: the convergence of the discrete problem (3.4) with initial guess $\boldsymbol{\alpha}_{int}^b$ is faster than the one computed with $\boldsymbol{\alpha}_{int}^a$. Moreover, the initial configurations lead us to two different local minimizers: the limit solution thus depends on the initial data. Figure 8 shows the approximate field for three time instances $t = 0.0125, 0.5, 1$ computed with initial guesses $\boldsymbol{\alpha}_{int}^a$ (top) and $\boldsymbol{\alpha}_{int}^b$ (bottom). Here, the magnitude of magnetic force $|\nabla|\boldsymbol{H}|^2|$ and the magnetic force vectors restricted to $D_{1,t}$ are depicted. From Figures 6 (right) and 7 (left) we notice a similar behavior for the intensities at initial times, thus in Figure 8 we observe an analogous magnetic force for both solutions at $t = 0.0125$. In both cases, the magnetic force is close to $\mathbf{f}_1$ in $D_{1,t}$ as expected, whence about constant, whereas it is quite far from constant in the entire domain.

Next, we approximate the vector field $\mathbf{f}_2$ defined on $D_{2,t}$. Figure 9 shows the initial guess computed by Algorithm 1 and the vector intensities $(\bar{\alpha}_{i,\tau})_{i=1}^8$ solutions to the minimization problem (3.4). The magnetic force is shown for three time instances $t = 0.0125, 0.5, 1$ in Figures 10. Here, the magnitude of magnetic force (in the background) and the magnetic force directions represented by arrows are depicted. The top figures illustrate the normalized magnetic force in Ω, but in the bottom figures the field is restricted to D_t. It is well-known that the magnetic forces on the boundary of the domain Ω are much higher than inside Ω. Thus making it difficult to approximate the magnetic force when D_t is close to the boundary. In fact, as we notice in the previous example, such high forces may lead to inferior approximation of the vector field $\mathbf{f}$. The optimization problem overcomes this situation and we observe that the optimal intensity $\bar{\boldsymbol{\alpha}}_i$ due to i^{th} dipole, is smaller when D_t is in close proximity to the i^{th} dipole and $\mathbf{f}$ is pointing in a direction opposite to the dipole position. This can be seen in Figure 6 (right) and Figure 7 (left), where the intensities of dipole 5 is small when t is close to 0. We notice a similar behavior (small intensities) in Figure 9 (right) for dipoles 5, 3 and 1, for t close to 0, 0.5 and 1, respectively. From the previous figures it can be seen that

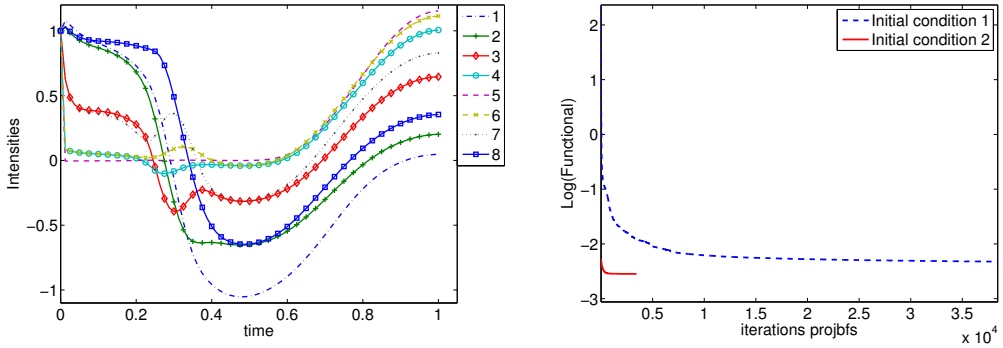


Figure 7: Optimal solution $\bar{\boldsymbol{\alpha}}_\tau = (\bar{\alpha}_{i,\tau})_{i=1}^8$ (left) to problem (3.4) computed with initial guess $\boldsymbol{\alpha}_{int}^a = \mathbf{1}$ and $\log(\mathcal{J}_\tau)$ computed at each optimization iteration with initial guess $\boldsymbol{\alpha}_{int}^a$ (dashed line) and $\boldsymbol{\alpha}_{int}^b$ (solid line) (right). The evolution of the intensities is shown for each dipole $i = 1, \ldots, 8$.

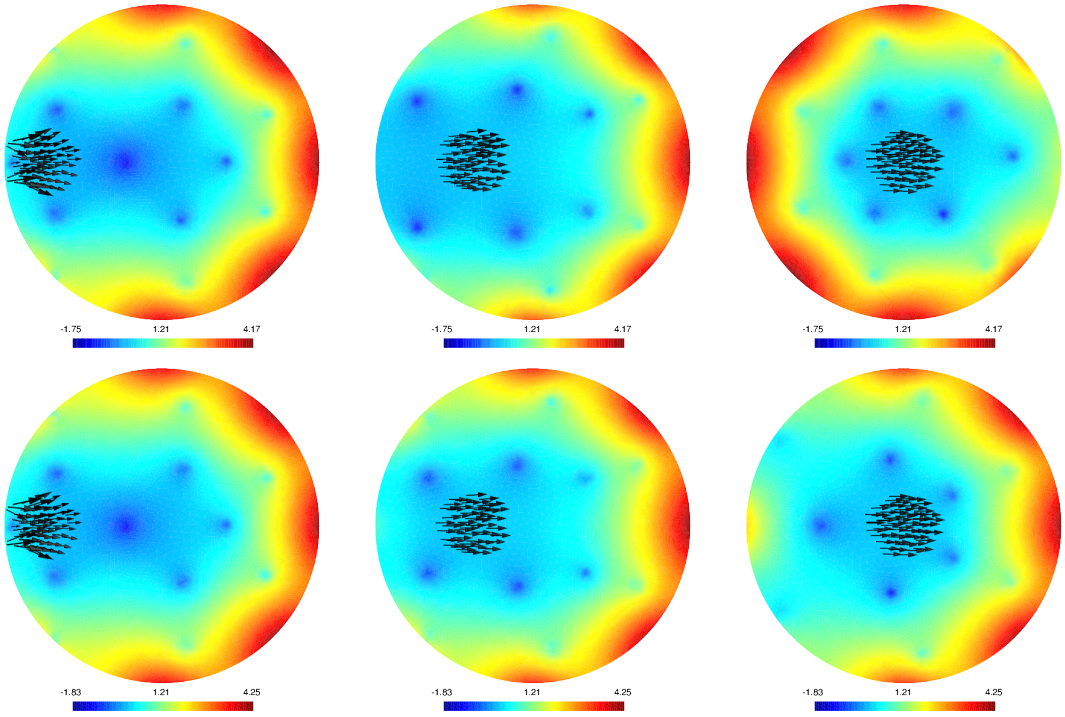


Figure 8: Magnetic force solution to the minimization problem with initial guess $\boldsymbol{\alpha}_{int}^a$ (top) and $\boldsymbol{\alpha}_{int}^b$ (bottom). Figures show the force at three different times $t = 0.0125, 0.5$ and 1 from left to right, respectively. For illustrative purposes the magnetic forces are depicted only in $D_{1,t}$ for the same time instances (directions shown by black arrows). The magnetic force magnitude $|\nabla|\boldsymbol{H}|^2|$ is shown by the background coloring on a logarithmic scale.

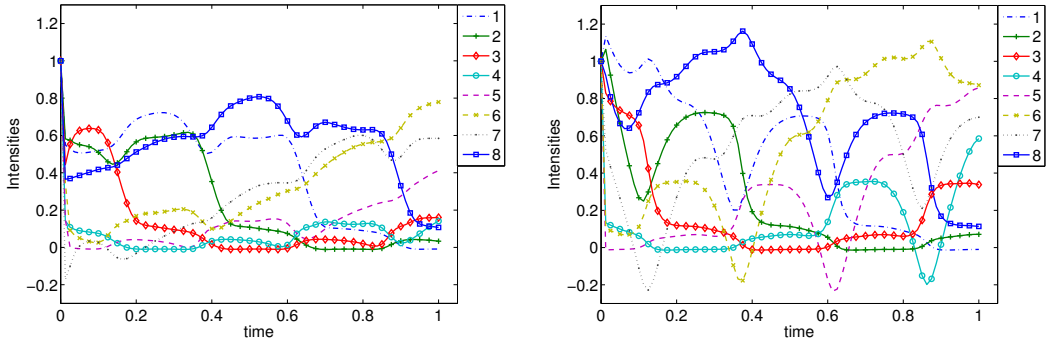


Figure 9: Initial guess $\boldsymbol{\alpha}_{int}^b$ computed by Algorithm 1 (left) and optimal solution $\bar{\boldsymbol{\alpha}}_\tau = (\bar{\alpha}_{i,\tau})_{i=1}^8$ to problem (3.4) with initial guess $\boldsymbol{\alpha}_{int}^b$ (right). The evolution of the intensities is shown for each dipole $i = 1, \ldots, 8$.

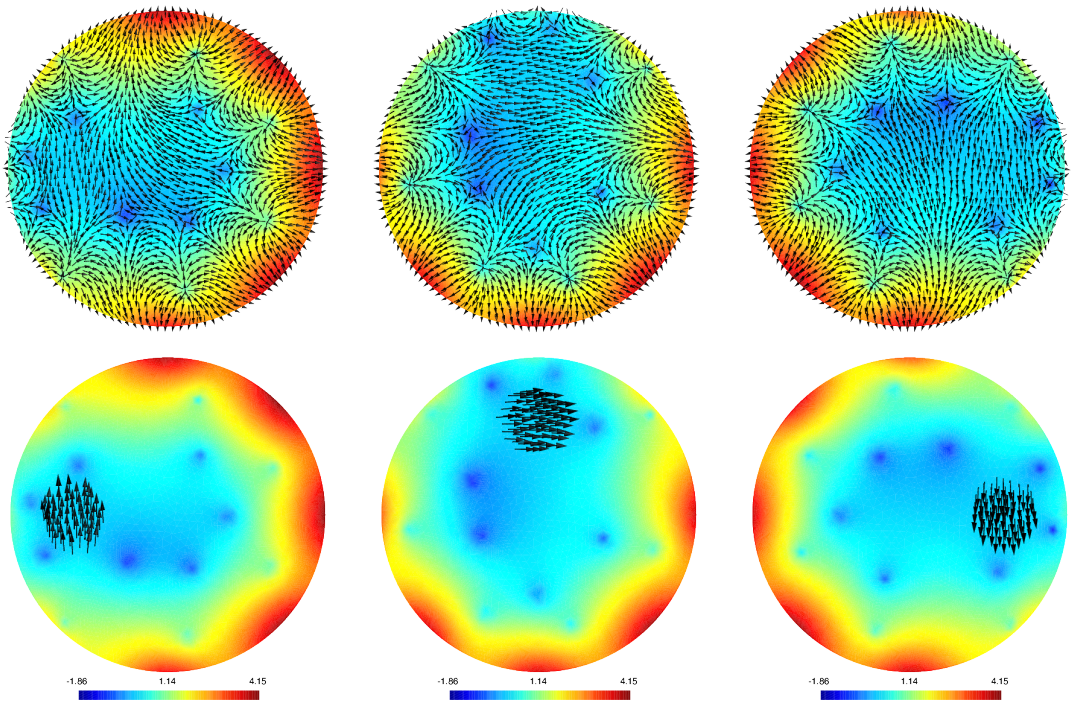


Figure 10: Magnetic force solution to the minimization problem with $D_{2,t}$ and vector field $\mathbf{f}_2$ (directions shown by black arrows). Top figure shows the force at three different times $t = 0.0125, 0.5$ and 1 from left to right, respectively. In the bottom figure the magnetic forces is defined only on $D_{2,t}$ for the same time instances. The magnetic force magnitude $|\nabla|\boldsymbol{H}|^2|$ is shown by the background coloring on a logarithmic scale.

our proposed minimization procedure produces a vector field that is close to the target field.

4.2 Problem 2: Optimal final time

We consider problem (3.16) with the curve $\mathcal{C}$ parameterized by

$$\boldsymbol{\rho}(s) = \boldsymbol{x}_I + s\frac{(\boldsymbol{x}_F - \boldsymbol{x}_I)}{\|\boldsymbol{x}_F - \boldsymbol{x}_I\|}, \qquad s \in [0, 0.75]$$

where the starting and end points are given by $\boldsymbol{x}_I = (0, -0.75)$ and $\boldsymbol{x}_F = (0, 0)$, respectively. For the arc length we consider a uniform discretization with $M = 80$ space intervals, namely, the space stepping is $\kappa = 0.75/M$. The upper and lower bounds characterizing the admissible set $\mathcal{U}_{ad}^{\kappa} \times \mathcal{V}_{ad}^{\kappa}$ are given by $(\boldsymbol{\alpha}_*, \boldsymbol{\alpha}^*, \theta_*, \theta^*) = (-1, 1, 10^{-10}, 10)$. As in the previous problem, we consider the following algorithm in order to obtain an initial guess for problem (3.16):

Algorithm 2 : Initialization algorithm

1: **Input:** $\boldsymbol{\alpha}_0$, θ_0, $\boldsymbol{\alpha}_*$, $\theta_*\boldsymbol{\alpha}^*$, θ^*, λ, κ, η, β, $\widehat{D}$, `tol`, $\boldsymbol{\rho}'$, $\widetilde{\boldsymbol{P}}_i^n$, $m = 1, \ldots, M$, $i = 1, \ldots, d$
2: Set $(\mathrm{x}^0, \mathrm{y}^0) := (\boldsymbol{\alpha}_0, \theta_0)$
3: **for** $m = 1, \ldots, M$ **do**
4: Solve for $(\mathbf{x}, \mathrm{y}) \in \mathbb{R}^{n_p+1}$

$$\min_{\substack{(\mathbf{x},\mathrm{y})\in\mathbb{R}^{n_p+1} \\ (\boldsymbol{\alpha}_*,\theta_*)\le(\mathbf{x},\mathrm{y})\le(\boldsymbol{\alpha}^*,\theta^*)}} F(\mathbf{x}, \mathrm{y})$$

$$F(\mathbf{x}, \mathrm{y}) = \frac{1}{2\mathrm{y}} \sum_{i=1}^{d} \|\mathbf{x}^\top \widetilde{\boldsymbol{P}}_i^n \mathbf{x} - \boldsymbol{\rho}'(m\kappa)\mathrm{y}\|_{\mathrm{L}^2(\widehat{D})}^2 + \frac{\beta}{\mathrm{y}} + \frac{\lambda}{2\kappa^2}|\mathbf{x} - \mathbf{x}^0|^2 + \frac{\eta}{2\kappa^2}|\mathrm{y} - \mathrm{y}^0|^2$$

with termination criterion: $|(\mathbf{x}, \mathrm{y}) - \mathrm{Proj}_{[\boldsymbol{\alpha}_*, \boldsymbol{\alpha}^*, \theta_*, \theta^*]}((\mathbf{x}, \mathrm{y}) - \nabla F(\mathbf{x}, \mathrm{y}))| < \mathtt{tol}$.
5: $\boldsymbol{\alpha}_{int}(n\kappa) = \mathbf{x}$, $\theta_I(n\kappa) = \mathrm{y}$
6: $\mathbf{x}^0 \leftarrow \mathbf{x}$, $\mathrm{y}^0 \leftarrow \mathrm{y}$
7: **end for**

We solve problem (3.16) for an initial condition $(\boldsymbol{\alpha}_0, \theta_0) = (10^{-6}, \ldots, 10^{-6}) \in \mathbb{R}^{n_p+1}$, $\beta = 10^{-1}$ and two set of cost parameters: $(\lambda_1, \eta_1) = (10^{-6}, 10^{-4})$ and $(\lambda_2, \eta_2) = (10^{-4}, 10^{-6})$. The initial guess is computed by using Algorithm 2. Figure 11 shows the evolution of velocity and intensity in term of arc length. The intensity plots (left and center) correspond to (λ_1, η_1) and(λ_2, η_2), respectively. On the other hand, the dotted line in the right figure shows the velocity when (λ_1, η_1) and the solid line corresponds to (λ_2, η_2). The computed values of velocity are $\theta_\kappa(t(s^m))$, $m = 1, \ldots, M$.

Since $\theta(\cdot) = \dfrac{ds}{dt}(\cdot)$, for $t \in [0, T_F]$, we compute the final time T_F by solving

$$s_F = \int_0^{T_F} \theta_\kappa(\tau)d\tau = \sum_{i=1}^{M} \int_{t^{i-1}}^{t^i} \left(\theta_\kappa^{i-1} + \left(\frac{\tau - t^{i-1}}{t^i - t^{i-1}} \right) (\theta_\kappa^i - \theta_\kappa^{i-1}) \right) d\tau,$$

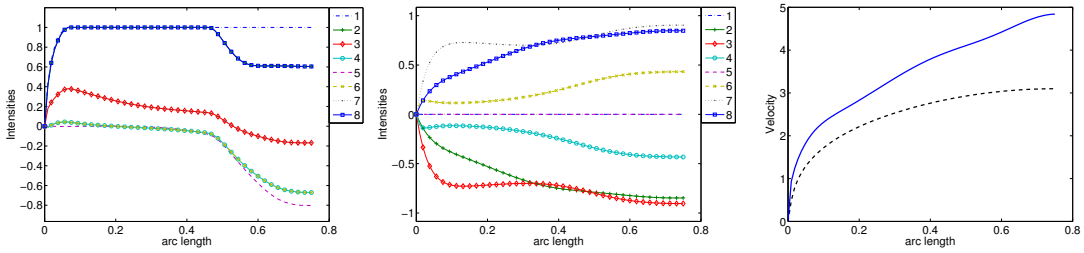


Figure 11: Intensity and velocity solutions to problem (3.16) with $\beta = 10^{-1}$. Evolution of the intensities $\{\boldsymbol{\alpha}_\kappa^i\}_{i=1}^8$ for parameters (λ_1, η_1) (left) and (λ_2, η_2) (center), and velocity θ_κ (right) for both parameters. The dotted line shows the velocity when (λ_1, η_1) and the solid line corresponds to (λ_2, η_2). The horizontal axis represents the arc length s of the curve $\mathcal{C}$ with $s_F = 0.75$.

where $t^i = t(s^i), i = 0, \ldots, M$. Because of the dependence on t^i, this equation has to be solved recursively:

$$
\begin{aligned}
s^1 &= \int_0^{t^1} \left(\theta_\kappa^0 + \frac{\tau}{t^1}(\theta_\kappa^1 - \theta_\kappa^0) \right) d\tau \longrightarrow t^1 = \frac{2s^1}{\theta_\kappa^1 + \theta_\kappa^0} \\
s^2 &= s^1 + \int_{t^1}^{t^2} \left(\theta_\kappa^1 + \left(\frac{\tau - t^1}{t^2 - t^1} \right) (\theta_\kappa^2 - \theta_\kappa^1) \right) d\tau \longrightarrow t^2 = \frac{2(s^2 - s^1)}{\theta_\kappa^2 + \theta_\kappa^1} + t^1 \\
&\vdots \quad \vdots \\
s^i &= s^{i-1} + \int_{t^{i-1}}^{t^i} \left(\theta_\kappa^{i-1} + \left(\frac{\tau - t^{i-1}}{t^i - t^{i-1}} \right) (\theta_\kappa^i - \theta_\kappa^{i-1}) \right) d\tau \longrightarrow t^i = \frac{2(s^i - s^{i-1})}{\theta_\kappa^i + \theta_\kappa^{i-1}} + t^{i-1}
\end{aligned}
\tag{4.1}
$$

for $i = 1, \ldots, M$. Therefore, the final time T_F is given by

$$
T_F = t^M = 2 \sum_{i=1}^{M} \frac{s^i - s^{i-1}}{\theta_\kappa^i + \theta_\kappa^{i-1}} = 2\kappa \sum_{i=1}^{M} \frac{1}{\theta_\kappa^i + \theta_\kappa^{i-1}}.
$$

Using the aforementioned formules we deduce that $T_F = 0.485$ when (λ_1, η_1) and $T_F = 0.337$ when (λ_2, η_2).

In order to increase the force in direction $\boldsymbol{\rho}' = (1, 0)^\top$ (cf. (2.13b)), in principle, it is sufficient to have only the dipole number one (see Figure 3) with maximum intensity $\bar{\boldsymbol{\alpha}}_1$ (cf. Figure 1, left). Indeed it is clear from Figure 11 (left) that the constraint $\bar{\boldsymbol{\alpha}}_1 = \boldsymbol{\alpha}^*$, is active for certain time instances. However, even though we can increase the magnetic force with only one dipole, it is safe to conclude that, for this example, even if we set $\bar{\boldsymbol{\alpha}} = \boldsymbol{\alpha}^*$ for all times, we do not achieve a uniform constant vector field (which is our goal). Then the remaining dipoles, which have nonzero intensities as well, contribute to attain this. On the contrary, Figure 11 (center) shows a different behavior. Here

the dipole $\bar{\boldsymbol{\alpha}}_1$ on the right has the same intensity as the dipole $\bar{\boldsymbol{\alpha}}_5$ on the left (close to 0), whereas the dipoles with the largest intensities are 3, 7 (at the center of $\emptyset$) and 2, 8 (on the right of $\emptyset$). Notice that the penalization $\lambda_1 = 10^{-6}$ of the cost functional leads to fast increasing values of dipoles intensities 1,2 and 8, which is not the case when $\lambda_2 = 10^{-4}$.

4.3 Application: Transport of a passive scalar

Magnetic drug targeting is an important application of ferrofluids where drugs, with ferromagnetic particles in suspension, are injected into the blood stream. The external magnetic field thus concentrates the drug to the most relevant areas, for example, solid tumors (see, for instance, [24]). We assume a concentration of magnetic nanoparticles confined in a domain $\widetilde{\Omega} \subset \mathbb{R}^d, d = 2, 3$. Let c be the drug concentration and $\boldsymbol{H}$ the magnetic field, then the evolution of c by the applied magnetic field is given by the following advection-diffusion model [13]:

$$\frac{\partial c}{\partial t} + \operatorname{div}\left(-A\nabla c + c\boldsymbol{u} + \gamma_1 c f(\boldsymbol{H})\right) = 0 \quad \text{in } \widetilde{\Omega} \times (0,T) \tag{4.2}$$

$$c = 0 \quad \text{on } \partial\widetilde{\Omega} \times (0,T) \qquad c(x,0) = c_0 \quad \text{in } \widetilde{\Omega} \tag{4.3}$$

$$\mathbf{curl}\, \boldsymbol{H} = \mathbf{0} \quad \text{in } \widetilde{\Omega} \qquad \operatorname{div}(\mu \boldsymbol{H}) = 0 \quad \text{in } \widetilde{\Omega} \tag{4.4}$$

where A is a diffusion coefficient matrix, $\boldsymbol{u}$ is a fixed velocity vector and f is the *Kelvin force* depending on $\boldsymbol{H}$ (cf (1.1)). If the magnetic susceptibility χ is independent of $\boldsymbol{H}$, then $f(\boldsymbol{H}) = \gamma_2 \mu_0 \chi \nabla |\boldsymbol{H}|^2$ where γ_1 and γ_2 are constitutive constants with different units and μ_0 denotes the magnetic permeability.

Under the principle of magnetic drug delivery, we aim to move an initial concentration c_0 of drugs from one subdomain to another (desired location) using the magnetic force while minimizing the spreading. In this example we focus on "magnetic injection" of the concentration away from the boundary. The two fundamental units that determine the evolution of concentration c are transport and diffusion (cf. (4.2)). Given the variability of the magnetic force in $\emptyset$ (see, Figures 10 (top)), the major challenges are: to generate the appropriate magnetic force to move the concentration to a desired location and to control the spreading due to the diffusion in (4.2).

Indeed, we can overcome the first of these challenges by using the "almost uniform" magnetic force generated using magnetic dipoles in the previous two examples. Recall that D_t moves along a pre-specified curve $\mathcal{C}$. In fact, in our computations we notice that the magnetic force in D_t helps in minimizing the spread of c as well.

To fix ideas, we set $\widetilde{\Omega} := \Omega \subset \mathbb{R}^2$ be a ball of unit radius centered at $(0,0)$ and the dipole configuration is the same as in the previous examples. We assume that c_0 is as in Figure 12 (left), and lies inside a ball centered at $(-0.75, 0)$ with radius 0.2 (see Figure 12 (left)). We also set final time $T = 1$. For simplicity we assume $\gamma_1 = \gamma_2 = \mu_0 = \chi = 1$, $\boldsymbol{u} = \mathbf{0}$. In order to further reduce the spread we choose a small diffusion coefficient, in particular, we set $A = \varepsilon \mathbb{I}$, with $\varepsilon = 10^{-5}$.

We consider piecewise linear functions on simplicial meshes to approximate (4.2)–(4.3). However, it is well–known that the standard finite element method yields solution

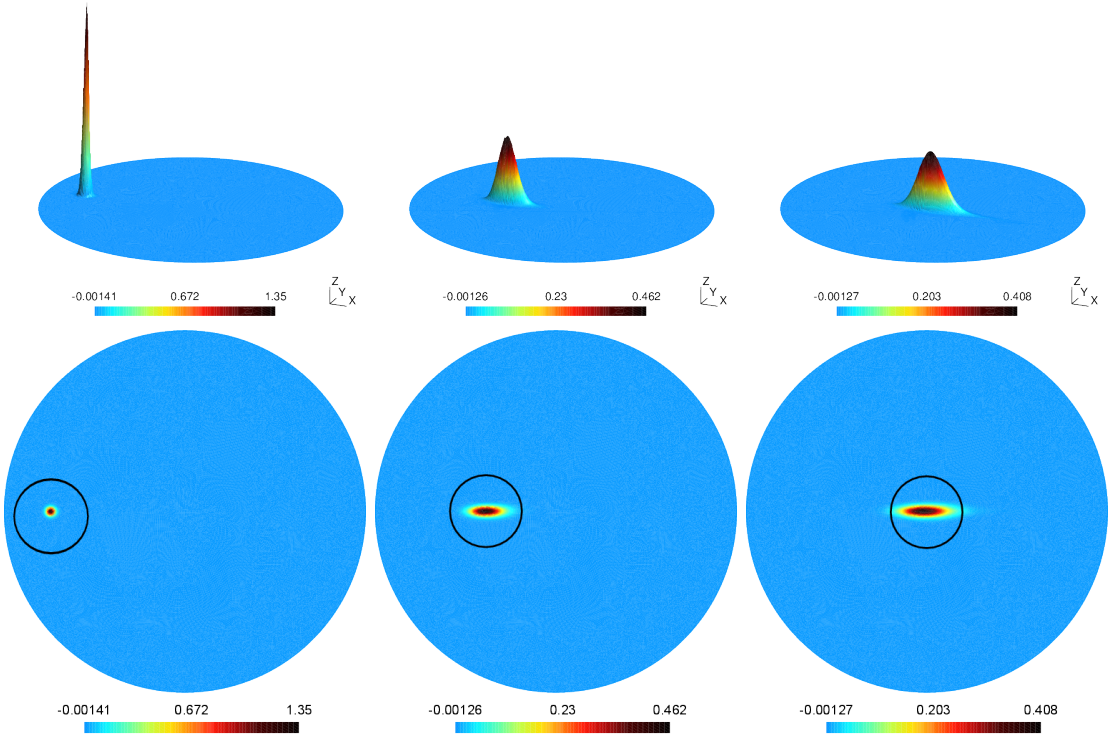


Figure 12: Evolution of the concentration in Ø and moving domain $D_{1,t}$ (circle) at times $t = 0, 0.5, 1$ s. $\varepsilon = 10^{-5}$ with two different views.

oscillations when $\varepsilon \ll |f(\boldsymbol{H})|$. A possible remedy is to add an artificial term to stabilize the numerical scheme. We use the so–called SUPG technique (see, for instance, [4]). Let $f(\boldsymbol{H}) = \nabla|\boldsymbol{H}|^2$ as computed in Section 4.1 by solving (3.4) $\mathbf{f} = \mathbf{f}_1 = (1, 0)$. Then we solve (4.2)-(4.3) for c.

Figure 12 shows the evolution of the concentration for three times instances.

From Figure 12, we notice that most part of the concentration c is confined in $D_{1,t}$ (denoted by the smaller circle) for all times. Indeed, our approach minimizes spreading and prevents concentration from reaching $\partial\Omega$. Otherwise, part of the concentration could be transported to the boundary where the closest (active) dipole is positioned, which is not our goal. Figure 12 illustrate that the concentration moves from the initial configuration and reaches at center of Ø.

References

[1] H. Antil, M. Hintermueller, R. H. Nochetto, T. M. Surowiec, and D. Wegner. Finite horizon model predictive control of electrowetting on dielectric with pinning. *Interface and Free Boundaries (to appear)*, 2016.

[2] G. Braides. Local minimization, variational evolution and Γ-convergence. In *Lectute Notes in Mathematics*. Springer, 2013.

[3] H. Brezis. *Functional Analysis, Sobolev Spaces and Partial Differential Equations*. Springer, 2011.

[4] A. Brooks and T. Hughes. Streamline upwind/Petrov-Galerkin formulations for convection dominated flows with particular emphasis on the incompressible Navier-Stokes equations. *Computer Methods in Applied Mechanics and Engineering*, 32:199–259, 1982.

[5] E. Casas and F. Tröltzsch. Error estimates for the finite-element approximation of a semilinear elliptic control problem. *Control Cybernet.*, 31:695–712, 2002. Well-posedness in optimization and related topics (Warsaw, 2001).

[6] C. Corot, P. Robert, J.-M. Idée, and M. Port. Recent advances in iron oxide nanocrystal technology for medical imaging. *Advanced Drug Delivery Reviews*, 58(14):1471 – 1504, 2006.

[7] G. Dal Maso. *An introduction to Γ-convergence*. Progress in Nonlinear Differential Equations and their Applications, 8. Birkhäuser Boston, Inc., Boston, MA, 1993.

[8] Anthony HB de Vries, Bea E Krenn, Roel van Driel, and Johannes S Kanger. Micro magnetic tweezers for nanomanipulation inside live cells. *Biophysical journal*, 88(3):2137–2144, 2005.

[9] J. Dobson. Gene therapy progress and prospects: Magnetic nanoparticle-based gene delivery. *Gene Ther*, 13:283–287, 2006.

[10] T.W.R. Fountain, P.V. Kailat, and J.J. Abbott. Wireless control of magnetic helical microrobots using a rotating-permanent-magnet manipulator. In *Robotics and Automation (ICRA), 2010 IEEE International Conference on*, pages 576–581, 2010.

[11] E. P. Furlani and X. Xue. A model for predicting field-directed particle transport in the magnetofection process. *Pharmaceutical Research*, 29(5):1366–1379, 2012.

[12] M.A.M. Gijs, F. Lacharme, and U. Lehmann. Microfluidic applications of magnetic particles for biological analysis and catalysis. *Chem. Rev.*, 110(3):1518–1563, 2010.

[13] A. D. Grief and G. Richardson. Mathematical modelling of magnetically targeted drug delivery. *Journal of Magnetism and Magnetic Materials*, 293:455 – 463, 2005. Proceedings of the Fifth International Conference on Scientific and Clinical Aplli-cations of Magnetic Carriers.

[14] M. Hintermüller, K. Ito, and K. Kunisch. The primal-dual active set strategy as a semismooth newton method. *SIAM J. on Optimization*, 13(3):865–888, August 2002.

[15] M. Hinze and A. Kauffmann. On a distributed control law with an application to the control of unsteady flow around a cylinder. In *Optimal Control of Partial Differential Equations*, volume 133 of *ISNM International Series of Numerical Mathematics*, pages 177–190. Birkhäuser Basel, 1999.

[16] B. G. Hosu, K. Jakab, P. Bánki, F. I. Tóth, and G. Forgacs. Magnetic tweezers for intracellular applications. *Review of Scientific Instruments*, 74(9):4158–4163, 2003.

[17] A. Jordan, P. Wust, H. Fähling, W. John, A. Hinz, and R. Felix. Inductive heating of ferrimagnetic particles and magnetic fluids: physical evaluation of their potential for hyperthermia. *Int J Hyperthermia*, 9:51 – 68, 1993.

[18] C. T. Kelley. *Iterative methods for optimization*, volume 18 of *Frontiers in Applied Mathematics*. Society for Industrial and Applied Mathematics (SIAM), Philadelphia, PA, 1999.

[19] A. Komaee and B. Shapiro. Magnetic steering of a distributed ferrofluid spot towards a deep target with minimal spreading. In *Decision and Control and European Control Conference (CDC-ECC), 2011 50th IEEE Conference on*, pages 7950–7955, Dec 2011.

[20] M.P. Kummer, J.J. Abbott, B.E. Kratochvil, R. Borer, A. Sengul, and B.J. Nelson. OctoMag: An electromagnetic system for 5-DOF wireless micromanipulation. *Robotics, IEEE Transactions on*, 26:1006–1017, 2010.

[21] U. Lehmann, S. Hadjidj, V.K. Parashar, C. Vandevyver, A. Rida, and M.A.M. Gijs. Two-dimensional magnetic manipulation of microdroplets on a chip as a platform for bioanalytical applications. *Sensors and Actuators B: Chemical*, 117(2):457 – 463, 2006.

[22] J.K. Lim, S. P. Yeap, and S. C. Low. Challenges associated to magnetic separation of nanomaterials at low field gradient. *Separation and Purification Technology*, 123:171 – 174, 2014.

[23] A. S. Lübbe, C. Alexiou, and C. Bergemann. Clinical applications of magnetic drug targeting. *Journal of Surgical Research*, 95(2):200 – 206, 2001.

[24] AS. Lübbe, C. Bergemann, H. Riess, F. Schriever, P. Reichardt, K. Possinger, M. Matthias, B. Dörken, F. Herrmann, and R. Gürtler. Clinical experiences with magnetic drug targeting: A phase I study with 4'-Epidoxorubicin in 14 patients with advanced solid tumors. *Cancer Research*, 56(20):4686–4693, 1996.

[25] A. W. Mahoney and J.J. Abbott. Managing magnetic force applied to a magnetic device by a rotating dipole field. *Applied Physics Letters*, 99, 2011.

[26] K. Maier-Hauff, F. Ulrich, D. Nestler, H. Niehoff, P. Wust, B. Thiesen, and A. Jordan. Efficacy and safety of intratumoral thermotherapy using magnetic iron-oxide nanoparticles combined with external beam radiotherapy on patients with recurrent glioblastoma multiforme. *Journal of Neuro-Oncology*, 103:317–324, 2011.

[27] P.H. Meyers, F. Cronic, and C.M. Nice. Experimental approach in the use and magnetic control of metallic iron particles in the lymphatic and vascular system of dogs as a contast and isotopic agent. *Am. J. Roentgenol. Radium Ther. Nucl. Med.*, 90:1068–1077, 1963.

[28] B. J. Nelson, I. K. Kaliakatsos, and J.J. Abbott. Microrobots for minimally invasive medicine. *Annual Review of Biomedical Engineering*, 12:55–85, 2010.

[29] A.J. Petruska and J.J. Abbott. Optimal permanent-magnet geometries for dipole field approximation. *Magnetics, IEEE Transactions on*, 49:811–819, 2013.

[30] R. E. Rosensweig. *Ferrohydrodynamics*. Dover Publications, 1997.

[31] R. E. Rosensweig. Basic equations for magnetic fluids with internal rotations. In *Ferrofluids*, volume 594 of *Lecture Notes in Physics*, pages 61–84. Springer Berlin Heidelberg, 2002.

[32] A. Sarwar, R. Lee, D.A. Depireux, and B. Shapiro. Magnetic injection of nanoparticles into rat inner ears at a human head working distance. *Magnetics, IEEE Transactions on*, 49:440–452, 2013.

[33] U. Schillinger, T. Bril, C. Rudolph, S. Huth, S. Gersting, F. Krötz, J. Hirschberger, C. Bergemann, and C. Plank. Advances in magnetofection–magnetically guided nucleic acid delivery. *Journal of Magnetism and Magnetic Materials*, 293(1):501 – 508, 2005.

[34] B. Shapiro, K. Dormer, and I. B. Rutel. A two-magnet system to push therapeutic nanoparticles. *AIP Conference Proceedings*, 1311:77–88, 2010.

[35] A. Solanki, J. D. Kim, and K.-B. Lee. Nanotechnology for regenerative medicine: nanomaterials for stem cell imaging. *Nanomedicine*, 3(4):567–578, 2008.

[36] C. Sun, J. S. H. Lee, and M Zhang. Magnetic nanoparticles in MR imaging and drug delivery. *Advanced Drug Delivery Reviews*, 60(11):1252 – 1265, 2008.

[37] F. Tröltzsch. *Optimal Control of Partial Differential Equations: Theory, Methods and Applications*. Grad. Stud. Math. 112, AMS, Providence, 2010.

[38] J. Zeng, Y. Deng, P. Vedantam, T-R. Tzeng, and X. Xuan. Magnetic separation of particles and cells in ferrofluid flow through a straight microchannel using two offset magnets. *Journal of Magnetism and Magnetic Materials*, 346(0):118 – 123, 2013.